A Robust Predictive Control Approach for Underwater Robotic Vehicles

Shahab Heshmati-Alamdari, George C. Karras, Panos Marantos, and Kostas J. Kyriakopoulos.

***Abstract*—This work presents a robust Nonlinear Model Predictive Control (NMPC) scheme for autonomous navigation of underwater robotic vehicles operating in a constrained workspace including static obstacles. In particular, the purpose of the controller is to guide the vehicle towards specific way points with guaranteed input and state constraints. Various constraints such as: obstacles, workspace boundaries, predefined upper bounds for the velocity of the robotic vehicle as well as thruster saturations are considered during the control design. Moreover, the proposed control scheme is designed at dynamic level and incorporates the full dynamics of the vehicle in which the ocean currents are also involved. Hence, taking the thrusts as the control inputs of the robotic system and formulating them accordingly, the vehicle exploits the ocean current dynamics, when these are in favor of the way-point tracking mission, resulting in reduced energy consumption by the thrusters. The robustness of the closed-loop system against parameter uncertainties has been analytically guaranteed with convergence properties. The performance of the proposed control strategy is experimentally verified using a 4 Degrees of Freedom (DoF) underwater robotic vehicle inside a constrained test tank with sparse static obstacles.**

***Index Terms*—Autonomous Underwater Vehicles, Marine Robotics, Model Predictive Control.**

I. Introduction

During the last decades, considerable progress has been made in the field of unmanned marine vehicles, with a significant number of positive results in a variety of marine activities [1]. Applications such as ocean forecasting, pollution management, ecosystem monitoring, underwater inspection and surveillance, marine resource utilization and oceanography are indicative examples of applications that require the underwater robots to operate under various constraints and increased level of autonomy and endurance [2].

On the design side, the endurance of an underwater system can be increased by improving the energy storage units (e.g., larger capacity batteries) [3] or reducing the vehicle's drag by design [4]. However, such approaches may solve partially the problem, due to current technology limitations, design constraints and reduced payload capabilities of the vehicle. Therefore, alternative approaches for energy reduction may considered. In general, the energy intake of an underwater vehicle is divided in two parts: i) the hotel load which is defined as the energy consumption of the on-board computers, processing effort, instrumentation and communication devices, and ii) the energy used by the propulsion system (e.g thrusters) [2]. The hotel load reduction can be achieved by employing low power devices and lean algorithms that do not require significant processing effort. On the other hand, the optimization of the thrust energy consumption, is mainly a path planning problem where the vehicle must reach the desired goal in an energy optimal manner.

Energy minimization via mission planning has been studied in the past and still remains an open research issue for the underwater robotics community. The ocean currents may significantly affect the vehicle motion and must be taken under consideration in the control design [5]. The importance of utilizing ocean currents in underwater vehicle operation was emphasized in [6], where a genetic algorithm planner was proposed for the design of a path with minimum energy requirements. In [7], the authors proposed a path planning method for an Autonomous Underwater Vehicle (AUV) based on the A^* search algorithm notion. In [8], an A^* energy efficient framework was proposed under the consideration of quasi-static ocean current information and constant thrust power. In [9], an A^* algorithm with energy based cost function was presented. Moreover, in [10], an A^* search was employed in order to design a continuous path, where the ocean currents were incorporated as quadratic drag force terms.

Alternative methods for the path planning of underwater vehicles are based on Rapidly Exploring Random Trees (RRTs) [11], where the workspace is explored in order to navigate the robot uniformly. A similar method to obtain an obstacle free path for an AUV was employed in [12]. However, no sea currents were taken under consideration during the design of the algorithm. In [13], RRTs were combined with A^* in order to generate feasible and energy optimized paths for gliders. The majority of the aforementioned planning techniques are based on off–line optimization schemes, which consider static or quasi–static operational environments. Their output is often a set of way-points or trajectories, which are optimal with respect to the energy consumption, while satisfy certain environmental constraints.

However, in real–time missions, the vehicle operates in a partially known and dynamic environment where the knowledge of the operating workspace is constantly updated on–line via the vehicle's on–board sensors (e.g multi beam imaging sonars, on-line ocean current estimators). In these cases, the underwater vehicle must re-calculate its path on–line according to possible environmental changes (i.e., new obstacles, other vehicles or humans operating in proximity etc.). More details regarding the open problems on underwater robotics path planning, can be found in [2] and [5] and the papers quoted therein.

Shahab Heshmati-alamdari is with the Division of Decision and Control Systems, School of Electrical Engineering and Computer Science, KTH Royal Institute of Technology, Stockholm, Sweden. G. C. Karras, P. Marantos and K. J. Kyriakopoulos are with the Control Systems Lab, School of Mechanical Engineering, National Technical University of Athens, Greece. Emails: shaha@kth.se, {karrasg,marantos,kkyria@mail.ntua.gr}. (Corresponding author: Shahab Heshmati-alamdari).

This work was supported by the Knut och Alice Wallenberg Academy (KAW) Fellow 2015.0216.

On the other hand, motion control of underwater vehicles is a highly nonlinear problem, where multiple input and state constraints are imposed to the system. Classical approaches such as local linearization and input-output decoupling have been used in the past to design motion controllers for underwater vehicles [14]. Nevertheless, the aforementioned methods yielded poor closed loop performance and the results were local, around only certain selected operating points. Output feedback linearization [15]–[17] is an alternative approach which however is not always possible. Moreover, based on a combined approach involving Lyapunov theory and backstepping, various model-based non-linear controllers have been proposed in the literature requiring a very accurate knowledge of the vehicle dynamic parameters, which in most cases is quite difficult to obtain [18]–[25]. More specifically, in [18], the authors proposed a cascade control strategy that consists of a kinematic control law that aims at tracking a desired trajectory and a dynamical control law, based on the backstepping technique, that tracks the desired velocity control signals. In [19], the authors proposed a nonlinear adaptive control law that drives an underwater vehicle along a sequence of desired way points. The controller is designed initially at the kinematic level and subsequently, employing the integrator backstepping technique, is extended to the dynamical model. However, the effect of ocean currents either is assumed to be known or an exponential observer is adopted for its estimation, thus increasing the design complexity. In [20], the authors proposed a tracking controller by employing integral backstepping technique. Nevertheless, the effect of the second hydrodynamic damping force was ignored. In [21], a model based output feedback control approach is proposed for a slender–body underwater vehicle. In [22], a position tracking controller for underwater vehicles was presented. The authors assumed that the motion of the vehicle is affected by constant, unknown ocean currents and designed an observer to estimate them. However, model uncertainties were not considered. In [23], a trajectory tracking controller for underactuated vehicles was designed based on the one-step ahead backstepping technique and the Lyapunov's direct method. In order to avoid the geometric singularities in the kinematic model, a combination of the Euler angles and unit-quaternion representation was adopted. However, even though the effect of sea currents was considered, the inherent uncertainties of the dynamic model were ignored. Finally, a path following and trajectory tracking control scheme for underactuated vehicles was proposed in [24], based on previous work in [25], resulting in a more smooth spatial convergence and a more tight temporal performance.

Dynamic model uncertainties of underwater robotic vehicles have been mainly compensated by employing adaptive control techniques [26], [27]. In [28], employing non smooth and homogeneity tools, an adaptive finite time tracking control approach has been developed for robust trajectory tracking of marine vehicles. In [29], the authors extended their previous work in [30], by proposing an adaptive control approach for an underwater robotic vehicle in presence of model uncertainties. However, owing to the sensitivity of the aforementioned controllers on unknown parameters, their capability in a real time experiment remains questionable. Additionally, experimental results employing an adaptive controller were presented in [31], where a priori knowledge of the dynamic parameters was requested. Furthermore, based on switching control strategies and backstepping techniques, a hybrid parameter adaptation law was presented in [32], [33], where the effect of external disturbances and un-modeled dynamics were not considered. Sliding mode theory was an alternative method used in the past to deal with dynamic parameters' uncertainties [34]–[40]. However, control input chattering is the main disadvantage of the aforementioned control strategies which may result in undesirable high frequency dynamics. Finally, adaptive neural network [41]–[46], learning [47]–[50] and fuzzy control [51]–[55] approaches have been proposed in literature for the motion control of underwater robotic vehicles. The aforementioned control strategies exploit the universal approximation capabilities of neural network and fuzzy system structures, but unfortunately, yield inevitably reduced levels of robustness against modeling imperfections [56]. In this spirit, approximating/estimating structures were introduced [57], [58], at the same time an increase of the complexity of the proposed control schemes was observed, in the sense that extra adaptive parameters have to be updated, thus making their implementation on fast embedded control systems difficult.

In addition, by employing all of the aforementioned motion control strategies, it is not always feasible or straightforward to incorporate input (generalized body forces/torques or thrust) and state (3D obstacles, velocities) constraints into the vehicle's closed-loop motion. In that sense, the motion control problem of underwater robots continues to pose considerable challenges to system designers, especially in view of the high-demanding missions envisioned by the marine industry (e.g., ship hull inspection, surveillance of oil platforms, cable installation and tracking, etc.).

Fig. 1: Experimental setup and problem formulation: the purpose of the controller is to guide the vehicle towards desired way points inside a constrained workspace including sparse obstacles.

In this context, Nonlinear Model Predictive Control (NMPC) [59], can be considered an ideal approach for complex underwater missions, as it is able to combine motion planning, obstacle avoidance and workspace restrictions, while handling efficiently input and state constraints. A sampling based Model Predictive Control scheme was proposed in

[60] for motion control of underwater vehicles in presence of constraints. A depth control strategy for an over-actuated hover-capable AUV based on Linear Model Predictive Control was presented in [61]. However, actuator limits were the only considered constraints of the system. In the same paper, the authors conclude that MPC is applicable for AUV control, while there are still open issues in topics such as robustness and estimation of the safe operating region (i.e., state constraints). In [62], the authors propose an MPC scheme in order to design an energy efficient path for a glider, by minimizing a cost function based on the consumed energy. However, only the kinematic model of the vehicle was considered, without taking into account any disturbances or noise of the ocean current profile. In order to optimize sawtooth paths for an AUV, an MPC scheme with least squares cost function was presented in [63]. Interesting results including estimated ocean wave profiles into an NMPC scheme, with an emphasis on real-time execution, were presented in [64]. However, the effect of noise and disturbance were not theoretically considered, but instead were presented through simulation testing. An MPC scheme with reduced dynamic model was presented in [65], where in order to avoid computational complexity, simplified linear models were considered for the vertical and horizontal control of the vehicle. In the aforementioned studies, the validation of the proposed strategies was conducted via simulation tests. An experimental validation of a visually aided NMPC scheme for an underwater robotic system was presented in [66], where simple kinematic equations of the system were considered.

A. Contribution

In this work[1], a robust NMPC scheme for underwater robotic vehicles is presented. The purpose of the controller is to guide the vehicle towards specific way points inside a constrained workspace including obstacles (See Fig.1). Various constraints such as: sparse obstacles, workspace boundaries, control input saturation as well as predefined upper bounds of the vehicle velocity (requirements for several underwater tasks such as seabed inspection scenario, mosaicking etc.) are considered during the control design. The proposed scheme incorporates the full dynamics of the vehicle in which the ocean currents are also involved. The controller is designed in order to find optimal thrusts (i.e., minimum forces generated by the thrusters) required for minimizing the way point tracking error. Moreover, the control inputs calculated by the proposed approach are formulated in a way that the vehicle will exploit the ocean currents, when these are in favor of the way-point tracking mission, resulting in reduced energy consumption by the thrusters. The closed-loop system has analytically guaranteed stability and convergence properties. Finally, the performance of the proposed control strategy is experimentally verified using a 4 DoF underwater robotic vehicle operating inside a constrained test tank with obstacles. To the best of the authors knowledge and compared to the existing works in the literature, this is the first time where a NMPC scheme which incorporates the full dynamics of the vehicle is experimentally verified in a constrained workspace including sparse obstacles. Moreover, the proposed control strategy is more complete with respect to existing works, since it incorporates input (i.e., thrust) and state (e.g., 3D obstacles, velocities) constraints into the vehicle's closed-loop motion and combines simultaneously real–time motion planing and control of the underwater robotic vehicle while considers at the same time energy consumptions issues.

[1]A preliminary version of this work, in the absence of a detailed analysis of the methodology, including stability and robustness analysis, and enriched set of comparative experimental results was reported in [67].

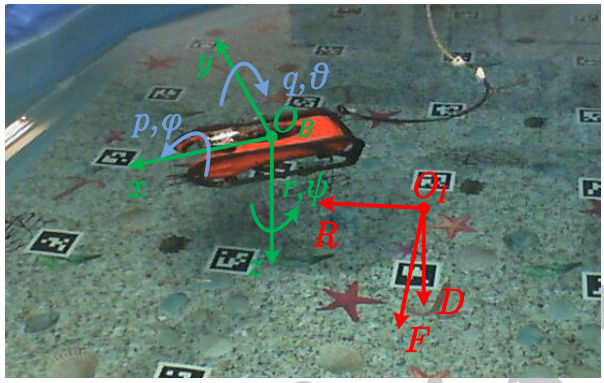

Fig. 2: Seabotix LBV150 ROV. The inertial frame ($\mathcal{I}$) and body-frame ($\mathcal{V}$) are indicated in red and green color respectively. The under-actuated DoFs are also depicted in blue color.

The rest of the paper is organized as follows: In Section-II, the modeling of the underwater vehicle along with the verbal description of the problem statement are presented. An analytical description of the proposed method including: i) the mathematical formulation of the problem, ii) the proposed control strategy and iii) the robust stability analysis are presented in Section-III. The efficiency of the proposed approach is illustrated in Section-IV via a set of experimental results. Finally, Section-V concludes the paper.

II. PRELIMINARIES AND PROBLEM FORMULATION

A. Notation

In this work, the vectors are denoted with lower bold letters whereas the matrices by capital bold letters. Given two sets A and $B \subset \mathbb{R}^n$, the Minkowski addition set C of two sets A and B is defined as: $C = A \oplus B = \{\boldsymbol{a} + \boldsymbol{b} : \boldsymbol{a} \in A, \boldsymbol{b} \in B\}$. The Pontryagin difference set P of two sets A and B is defined as $P = A \sim B = \{\zeta \in \mathbb{R}^n : \zeta + \xi \in A, \forall \xi \in B\}$. We define as $\mathcal{B}(\boldsymbol{c}, r) = \{\boldsymbol{x} \in \mathbb{R}^3 : \|\boldsymbol{x} - \boldsymbol{c}\| \leq r\}$ the closed sphere with radius r and center $\boldsymbol{c}$. For a given set $A \subset \mathbb{R}^n$ we define as $\text{cl}(A), \text{int}(A)$ and $\partial S = \text{cl}(A) \backslash \text{int}(A)$ its closure, interior and boundary, respectively. Thus, we have $A = \text{int}(A) \cup \partial A$.

B. Mathematical Modeling

The prior step before analyze the proposed methodology is the presentation of the preliminary aspects of the modeling of underwater vehicles. Firstly, let us define a common body-fixed frame $\mathcal{V}$ attached to the vehicle center of gravity, as well as the inertial frame $\mathcal{I}$ as shown in Fig-2. The pose vector of the vehicle with respect to (w.r.t) the inertial frame $\mathcal{I}$ is denoted by $\boldsymbol{\eta} = \left[\boldsymbol{\eta_1^T}\ \boldsymbol{\eta_2^T}\right]^T \in \mathbb{R}^6$ including the position (i.e., $\boldsymbol{\eta_1} = [x\ y\ z]^T$) and orientation (i.e., $\boldsymbol{\eta_2} = [\phi\ \theta\ \psi]^T$) vectors.

The $\boldsymbol{v} = \begin{bmatrix}\boldsymbol{v_1^T} & \boldsymbol{v_2^T}\end{bmatrix}^T \in \mathbb{R}^6$ is the velocity vector of the vehicle expressed in fixed-body frame $\mathcal{V}$ and includes the linear (i.e., $\boldsymbol{v_1} = [u\ v\ w]^T$) and angular (i.e., $\boldsymbol{v_2} = [p\ q\ r]^T$) velocity vectors. In this work, we consider that the vehicle operates under the influence of bounded irrotational ocean currents w.r.t the inertial frame $\mathcal{I}$. An estimation of the ocean currents can be achieved by employing the data obtained from Naval Coastal Ocean Model (NCOM) [68] and Regional Ocean Model Systems (ROMS) [69]. However, an estimation of the ocean current could be achieved locally using an appropriate estimator [19], [70]. Thus, in the following analysis, we consider the effect of ocean currents during the control design, but we assume that these data are inaccurate and the uncertainties on the ocean current's profile should be handled during the robustness analysis. In this work, the bounded irrotational ocean current velocities w.r.t the inertial frame $\mathcal{I}$ is denoted by $\boldsymbol{v}_c^{\mathcal{I}} = [(\boldsymbol{v}_{c_1}^{\mathcal{I}})^T, \boldsymbol{0}_{1\times 3}]^T \in \mathbb{R}^6$ with $\boldsymbol{v}_{c_1}^{\mathcal{I}} = [u_c^{\mathcal{I}}, v_c^{\mathcal{I}}, w_c^{\mathcal{I}}]^T$ to be the vector of linear velocity terms. Therefore, we can define the vehicle velocity vector relative to the water expressed in body frame $\mathcal{V}$ as:

$$\boldsymbol{v}_r = \boldsymbol{v} - \boldsymbol{v}_c \tag{1}$$

Notice that the vector $\boldsymbol{v}_c = [u_c, v_c, w_c, \boldsymbol{0}_{1\times 3}]^T$ indicates the expression of the ocean currents with respect to the body frame $\mathcal{V}$. Without loss of generality, according to the standard underwater vehicles' modeling properties [71], assuming that the current velocity is slowly varying with respect to the inertial frame (e.g, $\frac{\partial \boldsymbol{v}_c^{\mathcal{I}}}{\partial t} \approxeq 0$), and the vehicle is operating at relative low speeds, the dynamic equations of the vehicle can be given as [71, eq:3.112-3.116]:

$$\dot{\boldsymbol{\eta}} = \boldsymbol{J}(\boldsymbol{\eta})\,\boldsymbol{v}_r + \boldsymbol{v}_c^{\mathcal{I}} \tag{2a}$$

$$\boldsymbol{M}\dot{\boldsymbol{v}}_r + \boldsymbol{C}(\boldsymbol{v}_r)\,\boldsymbol{v}_r + \boldsymbol{D}(\boldsymbol{v}_r)\boldsymbol{v}_r + \boldsymbol{g}(\boldsymbol{\eta}) = \boldsymbol{\tau}_{\mathcal{V}} \tag{2b}$$

where:

- $\boldsymbol{\tau}_{\mathcal{V}} = [X,\ Y,\ Z,\ K,\ M,\ N]^T \in \mathbb{R}^6$ is the total propulsion force/torque vector (i.e., the body forces and torques generated by the thrusters) applied on the vehicle and expressed in $\mathcal{V}$;
- $\boldsymbol{M} = \boldsymbol{M}_{RB} + \boldsymbol{M}_A$, where $\boldsymbol{M}_{RB} \in \mathbb{R}^{6\times 6}$ and $\boldsymbol{M}_A \in \mathbb{R}^{6\times 6}$ are the inertia matrix for the rigid body and added mass respectively;
- $\boldsymbol{C}(\boldsymbol{v}_r) = \boldsymbol{C}_{RB}(\boldsymbol{v}_r) + \boldsymbol{C}_A(\boldsymbol{v}_r)$, where $\boldsymbol{C}_{RB}(\boldsymbol{v}_r) \in \mathbb{R}^{6\times 6}$ and $\boldsymbol{C}_A(\boldsymbol{v}_r) \in \mathbb{R}^{6\times 6}$ are the coriolis and centripetal matrix for the rigid body and added mass respectively;
- $\boldsymbol{D}(\boldsymbol{v}_r) = \boldsymbol{D}_{quad}(\boldsymbol{v}_r) + \boldsymbol{D}_{lin}(\boldsymbol{v}_r)$, where $\boldsymbol{D}_{quad}(\boldsymbol{v}_r) \in \mathbb{R}^{6\times 6}$ and $\boldsymbol{D}_{lin}(\boldsymbol{v}) \in \mathbb{R}^{6\times 6}$ are the quadratic and linear drag matrix respectively;
- $\boldsymbol{g}(\boldsymbol{\eta}) \in \mathbb{R}^6$ is the hydrostatic restoring force vector;
- $\boldsymbol{J}(\boldsymbol{\eta}) = \begin{bmatrix} \boldsymbol{J}_1(\boldsymbol{\eta_2}) & \boldsymbol{0}_{3\times 3} \\ \boldsymbol{0}_{3\times 3} & \boldsymbol{J}_2(\boldsymbol{\eta_2}) \end{bmatrix}$ is the Jacobian matrix transforming the velocities from the body-fixed ($\mathcal{V}$) to the inertial ($\mathcal{I}$) frame, in which $\boldsymbol{J}_1(\boldsymbol{\eta_2}) \in SO(3)$ is the well known rotation matrix and $\boldsymbol{J}_2(\boldsymbol{\eta_2}) \in \mathbb{R}^{3\times 3}$ denotes the lumped transformation matrix;

Notice that the transformation from ocean current velocity defined in the inertial frame $\mathcal{I}$ (i.e., $\boldsymbol{v}_c^{\mathcal{I}}$) into body-fixed one (i.e., $\boldsymbol{v}_c$) is achieved using the transposed rotation matrix i.e., $\boldsymbol{v}_c = \boldsymbol{J}^T(\boldsymbol{\eta})\boldsymbol{v}_c^{\mathcal{I}}$ (See [71]). In (2), the total propulsion force/torque vector ($\boldsymbol{\tau}_{\mathcal{V}}$) is computed using the thruster allocator matrix which is formulated by the actuation geometry and properties of the underwater vehicle's thrusters. The vehicle used in this work is a 4 DoF Seabotix LBV150. It is equipped with 4 thrusters (i.e., Port (p_o), Starboard (s), Vertical (v_e), Lateral (l)), which are effective in Surge (X), Sway (Y), Heave (Z) and Yaw (N) motion. Thus, we can define a new thrust vector ($\boldsymbol{\tau} = [\tau_{p_o},\ \tau_s,\ \tau_{v_e},\ \tau_l]^T \in \mathbb{R}^4$) and the appropriate thruster allocator matrix ($\boldsymbol{T_A} \in \mathbb{R}^{4\times 4}$) such as:

$$\boldsymbol{\tau}_{LBV}^{\mathcal{V}} = \boldsymbol{T_A}\boldsymbol{\tau}, \tag{3}$$

where $\boldsymbol{\tau}_{LBV}^{\mathcal{V}}\,[X,\ Y,\ Z,\ N]^T \in \mathbb{R}^4$.

Remark 1: The vehicle used in this work is designed with meta-centric restoring forces in order to regulate roll and pitch angles. Thus, the angles ϕ, θ and angular velocities p and q are negligible and we can consider them to be equal to zero. Thus, from now on, we denote $\boldsymbol{\eta} = [x, y, z, \psi]^\top$ and $\boldsymbol{v} = [u, v, w, r]^\top$. The vehicle is symmetric about x - z plane and close to symmetric about y - z plane. Therefore, we can safely assume that motions in heave, roll and pitch are decoupled [71].

C. Problem Formulation

Herein, we address the problem under consideration:

Problem 1: Given an underwater vehicle with dynamics as described in (2), design a robust feedback control law for the autonomous guidance towards a set of way-points $\boldsymbol{\eta}_i^d,\ i = \{1, \ldots, n\}$, while guaranteeing the following specifications:

- Avoid the workspace boundaries and a limited set of obstacles within.
- Respect operational limitations in the form of state (e.g velocity bounds) and input (thrust saturation) constraints.
- The energy consumed by thrusters to be retained in a reduced level.

III. METHODOLOGY

In this Section, we present in detail the methodologies proposed in order to formulate the solution of Problem 1 as defined in Section II-C.

A. Geometry of Workspace

Consider an underwater vehicle which operates inside the workspace $\mathcal{W} \subset \mathbb{R}^3$ with boundaries $\partial\mathcal{W} = \{\boldsymbol{p} \in \mathbb{R}^3 : \boldsymbol{p} \in \text{cl}(\mathcal{W})\backslash\text{int}(\mathcal{W})\}$ and sparse obstacles located within. Without loss of generality, the robot and the obstacles can be modeled as spheres (i.e., we adopt the spherical world representation [72]). In this spirit, let $\mathcal{B}(\boldsymbol{\eta}_1, \bar{r})$ to be a closed sphere that completely surrounds the vehicle volume (main body and additional equipments). Moreover, the $\mathcal{M}$ static obstacles within the workspace are defined as closed spheres described by $\pi_m = \mathcal{B}(\boldsymbol{p}_{\pi_m}, r_{\pi_m}),\ m \in \{1, \ldots, \mathcal{M}\}$, where $\boldsymbol{p}_{\pi_m} \in \mathbb{R}^3$ is the center and the $r_{\pi_m} > 0$ the radius of the obstacle π_m. Additionally, based on the property of spherical

world [72], for each pair of obstacles $m, m' \in \{1, \ldots, \mathcal{M}\}$ the following inequality holds:

$$||\pi_m - \pi_{m'}|| > 2\bar{r} + r_{\pi_m} + r_{\pi'_m} \tag{4}$$

which intuitively means that the obstacles m and m' are disjoint in such a way that the entire volume of the vehicle can pass through the free space between them. Therefore, there exists a feasible trajectory $\boldsymbol{\eta}(t)$ for the vehicle that connects the initial configuration $\boldsymbol{\eta}(t_0)$ with $\boldsymbol{\eta}^d$ such as:

$$\mathcal{B}(\boldsymbol{\eta}_1(t), \bar{r}) \cap \{\mathcal{B}(\boldsymbol{p}_{\pi_m}, r_{\pi_m}) \cup \partial\mathcal{W}\} = \emptyset, \ m \in \{1, \ldots, \mathcal{M}\}$$

A graphical representation of the feasible trajectory is depicted in Fig. 3.

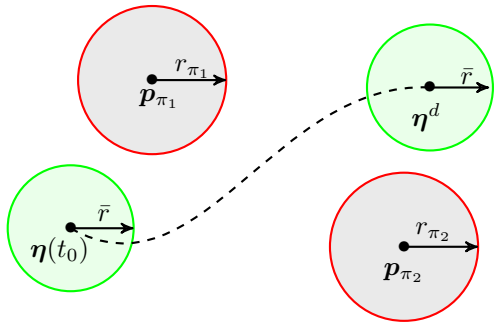

Fig. 3: Graphical representation of a feasible transition of the underwater vehicle from the initial position $\boldsymbol{\eta}(t_0)$ to the desired position $\boldsymbol{\eta}^d$. The underwater robotic vehicle in initial and desired configurations as well as the obstacles are indicated by green and red circles respectively. The feasible trajectory is indicated by dashed line.

B. Dynamical system

Due to the aforementioned assumptions and following standard simplifications due to symmetries in the mass configuration [71], the dynamic equation (2) for the vehicle under consideration, can be written in discrete-time form as:

$$\boldsymbol{x}_{k+1} = f(\boldsymbol{x}_k, \boldsymbol{\tau}_k) \Rightarrow \boldsymbol{x}_{k+1} = \boldsymbol{x}_k + \mathcal{A}(\boldsymbol{x}_k)dt + \mathcal{C}(\boldsymbol{\tau}_k)dt \tag{5}$$

where:

$$\mathcal{A}(\boldsymbol{x}_k) = \begin{bmatrix} u_{r_k}\cos(\psi_k) - v_{r_k}\sin(\psi_k) + u_c^{\mathcal{I}} \\ u_{r_k}\sin(\psi_k) + v_{r_k}\cos(\psi_k) + v_c^{\mathcal{I}} \\ w_{r_k} + w_c^{\mathcal{I}} \\ r_{r_k} \\ \frac{1}{m_{11}}(m_{22}v_{r_k}r_{r_k} + X_u u_{r_k} + X_{u|u|}|u_{r_k}|u_{r_k}) \\ \frac{1}{m_{22}}(-m_{11}u_{r_k}r_{r_k} + Y_v v_{r_k} + Y_{v|v|}|v_{r_k}|v_{r_k}) \\ \frac{1}{m_{33}}(Z_w w_{r_k} - m_{22}u_{r_k}v_{r_k} + Z_{w|w|}|w_{r_k}|w_{r_k}) \\ \frac{1}{m_{44}}((m_{11}-m_{22})u_{r_k}v_{r_k} + N_r r_{r_k} + N_{r|r|}|r_{r_k}|r_{r_k}) \end{bmatrix},$$

$$\mathcal{C}(\boldsymbol{\tau}_k) = \begin{bmatrix} \mathbf{0}_{4\times 1} \\ \boldsymbol{T_A}\boldsymbol{\tau}_k \end{bmatrix}$$

with $\boldsymbol{x_k} = [\boldsymbol{\eta}_k^T, \boldsymbol{v}_{r_k}^T]^T = [x_k,\ y_k,\ z_k,\ \psi_k,\ u_{r_k},\ v_{r_k},\ w_{r_k},\ r_{r_k}]^\top \in \mathbb{R}^8$ denotes the state vector at the time-step k which includes the position and orientation of the vehicle with respect to the inertial frame $\mathcal{I}$ and the relative linear and angular velocity of the vehicle with respect to the water. In addition, $m_{ii}, i = 1, \ldots, 4$ are the mass terms including added mass, $X_u,\ Y_v,\ Z_w,\ N_r\ < 0$ are the linear drag terms, $X_{u|u|},\ Y_{v|v|},\ Z_{w|w|},\ N_{r|r|}\ < 0$ are the quadratic drag terms, while dt denotes the sampling period. The control input of the system is $\boldsymbol{\tau}_k = [\tau_{p_k},\ \tau_{s_k},\ \tau_{v_k},\ \tau_{l_k}]^T \in \mathbb{R}^4$ consisting of the thrusters' forces. As mentioned previously, the ocean current profile induced to the dynamic model is inaccurate (i.e., in general, it is an estimation achieved by employing data from NCOM or ROMS) and consequently a difference between the real value of the current and the estimated one must be considered. The effect of these uncertainties can be considered as disturbances on the system (5). Thus, by $\boldsymbol{\delta_k} = [\mathbf{0}_{1\times 4},\ \delta_{u_k},\ \delta_{v_k},\ \delta_{w_k},\ \delta_{r_k}]^\top \in D \subset \mathbb{R}^8$ we present the effect of ocean current profile uncertainties on the system at the time step k, with D to be a compact set. Moreover, D is bounded by $||\boldsymbol{\delta_k}|| \leq \bar{\boldsymbol{\delta}}$. Furthermore, it is assumed that vehicle's dynamic parameters have been identified via a proper identification scheme. However some degree of uncertainty on dynamic parameters denoted by $\Delta f(\boldsymbol{x}_k, \boldsymbol{\tau}_k)$ should be considered. Taking into consideration the aforementioned disturbances that affect the vehicle, we are now ready to model the perturbed system as follows:

$$\begin{aligned} \boldsymbol{x}_{k+1} &= \tilde{f}(\boldsymbol{x}_k, \boldsymbol{\tau}_k) + \boldsymbol{\delta}_k = f(\boldsymbol{x}_k, \boldsymbol{\tau}_k) + \Delta f(\boldsymbol{x}_k, \boldsymbol{\tau}_k) + \boldsymbol{\delta}_k \\ &= f(\boldsymbol{x}_k, \boldsymbol{\tau}_k) + \boldsymbol{\gamma}_k + \boldsymbol{\delta}_k \end{aligned} \tag{6}$$

with:

$$\boldsymbol{\gamma}_k = \Delta f(\boldsymbol{x}_k, \boldsymbol{\tau}_k) \in \Gamma,\ ||\boldsymbol{\gamma}_k|| \leq \bar{\gamma}\ \forall \boldsymbol{x}_k \in X, \boldsymbol{\tau}_k \in T$$

where Γ is the compact set of uncertainties and $\bar{\gamma} \geq 0$ is a positive upper bound for this set. The equation (6) can be rewritten as:

$$\boldsymbol{x}_{k+1} = f(\boldsymbol{x}_k, \boldsymbol{\tau}_k) + \boldsymbol{w}_k \tag{7}$$

with $\boldsymbol{w}_k = \boldsymbol{\gamma}_k + \boldsymbol{\delta}_k \in W \subset \mathbb{R}^8$ as the result of adding uncertainties and external disturbances of the system. W is a compact set such that $W = D \oplus \Gamma$. Since the sets D and Γ are compact, W is also a compact set, bounded by $||\boldsymbol{w}_k|| \leq \bar{w}$ with $\bar{w} \triangleq \bar{\gamma} + \bar{\delta}$.

Remark 2: Notice that Eq. (7) is the actual dynamical equation of the system, since it contains the vector of disturbance effecting on the system. In this way, we consider Eq.(5) as the nominal model of the system, in which no disturbances are considered.

Property 1: The nominal model $f(\boldsymbol{x}, \boldsymbol{\tau})$ in eq.(5) is locally Lipschitz in X i.e., there is a positive Lipschitz constant $L_f < \infty$, such that for every $\boldsymbol{\tau} \in T$, $\|f(\boldsymbol{x}_1, \boldsymbol{\tau}) - f(\boldsymbol{x}_2, \boldsymbol{\tau})\| \leq L_f \|\boldsymbol{x}_1 - \boldsymbol{x}_2\|$.

C. Constraints

State Constraints:

In this work, we consider that the robot must avoid the obstacles and the workspace boundaries (test tank). Moreover, for the needs of several common underwater tasks (e.g., seabed inspection, mosaicking), the vehicle is required to move with relatively low speeds with upper bound denoted by the velocity vector $\boldsymbol{v}_p = [u_p\ v_p\ w_p\ r_p]^\top$. These requirements are captured by the state constraint set X of the system, given by:

$$\boldsymbol{x_k} \in X \subset \mathbb{R}^8 \tag{8}$$

which is formed by the following constraints:

$$u_p + v_p - |u_r + v_r| \geq 0 \tag{9a}$$
$$w_p - |w_r| \geq 0 \tag{9b}$$
$$r_p - |r_r| \geq 0 \tag{9c}$$
$$\mathcal{B}(\boldsymbol{\eta}_1(t), \bar{r}) \cap \{\mathcal{B}(\boldsymbol{p}_{\pi_m}, r_{\pi_m}) \cup \partial\mathcal{W}\} = \emptyset, \quad m \in \{1, \ldots, \mathcal{M}\} \tag{9d}$$

Input Constraints:
The actuation body forces and torques are generated by the thrusters. Thus, we define the control constraint set T as follows:

$$\boldsymbol{\tau}_k = [\tau_{p_{o_k}},\ \tau_{s_k},\ \tau_{v_{e_k}},\ \tau_{l_k}]^T \in T \subseteq \mathbb{R}^4 \tag{10}$$

These constraints are of the form $|\tau_{p_{o_k}}| \leq \bar{\tau}_{p_o}$, $|\tau_{s_k}| \leq \bar{\tau}_s$, $|\tau_{v_{e_k}}| \leq \bar{\tau}_{v_e}$ and $|\tau_{l_k}| \leq \bar{\tau}_l$, therefore we get $|||\boldsymbol{\tau}_k|| \leq \bar{T}$ where $\bar{T} = (\bar{\tau}_{p_o}^2 + \bar{\tau}_s^2 + \bar{\tau}_{v_e}^2 + \bar{\tau}_l^2)^{\frac{1}{2}}$ and $\bar{\tau}_{p_o}, \bar{\tau}_s, \bar{\tau}_{v_e}, \bar{\tau}_l \in \mathbb{R}_{\geq 0}$.

D. Control Design

The control objective is to guide the actual system (7) to a desired compact set around the way points $i = \{1, \ldots, n\}$ that includes the desired state ${}^i\boldsymbol{x}^d \triangleq [({}^i\boldsymbol{\eta}^d)^T, ({}^i\boldsymbol{v}_r^d)^T]^T = [{}^i x_d, {}^i y_d, {}^i z_d, {}^i \psi_d, {}^i u_d, {}^i v_d, {}^i w_d, {}^i r_d]^T \in X$, while respecting the state constraints (9a)-(9d) as well as the input constraints (10). A predictive controller is employed in order to achieve this task. In particular, at a given time instant k, the NMPC is assigned to solve an Optimal Control Problem (OCP) with respect to a control sequence $\boldsymbol{\tau}_f(k) \triangleq [\boldsymbol{\tau}(k|k), \boldsymbol{\tau}(k+1|k), \ldots, \boldsymbol{\tau}(k+N-1|k)]$, for a prediction horizon N. The OCP of the NMPC is given as follows:

$$\min_{\boldsymbol{\tau}_f(k)} J_N(\boldsymbol{x}_k, \boldsymbol{\tau}_f(k)) = \tag{11a}$$
$$\min_{\boldsymbol{\tau}_f(k)} \sum_{j=0}^{N-1} F(\hat{\boldsymbol{x}}(k+j|k), \boldsymbol{\tau}(k+j|k)) + E(\hat{\boldsymbol{x}}(k+N|k))$$

subject to:

$$\hat{\boldsymbol{x}}(k+j|k) \in X_j, \quad \forall j = 1, \ldots, N-1, \tag{11b}$$
$$\boldsymbol{\tau}(k+j|k) \in T, \quad \forall j = 0, \ldots, N-1, \tag{11c}$$
$$\hat{\boldsymbol{x}}(k+N|k) \in \mathscr{E}_f \tag{11d}$$

where $\mathscr{E}_f$ is the terminal set and F and E are the running and terminal cost functions, respectively. At time instant k, the solution of the OCP (11a)-(11d) is providing an optimal control sequence, denoted as:

$$\boldsymbol{\tau}_f^*(k) = [\boldsymbol{\tau}(k|k), \boldsymbol{\tau}(k+1|k), \ldots, \boldsymbol{\tau}(k+N-1|k)] \tag{12}$$

where the first control vector (i.e., $\boldsymbol{\tau}(k|k)$) is applied to the system. At the next time-step $k+1$, a new state measurement is received and the whole procedure is repeated again. The disturbance term $\boldsymbol{w}_k$ can cause discrepancies between the predicted state given from the nominal model (5) subject to a specific sequence of inputs and the actual state, given from (7) for the same sequence of inputs. In order to account for this mismatch we use the double subscript notation for the predicted state of system (5) inside the OCP of the NMPC:

$$\hat{\boldsymbol{x}}(k+j|k) = f(\hat{\boldsymbol{x}}(k+j-1|k), \boldsymbol{\tau}(k+j-1|k)) \tag{13}$$

where the vector $\hat{\boldsymbol{x}}(k+j|k)$ denotes the predicted state of the nominal system (5) at sampling time $k+j$ with $j \in \mathbb{Z}_{\geq 0}$. The predicted state is based on the measurement of the state $\boldsymbol{x}_k$ of the actual system at sampling time k (i.e., provided by the on–board navigation system), while applying a sequence of control inputs $[\boldsymbol{\tau}(k|k), \boldsymbol{\tau}(k+1|k), \ldots, \boldsymbol{\tau}(k+j-1|k)]$. It holds that $\hat{\boldsymbol{x}}(k|k) \equiv \boldsymbol{x}_k$. The cost function $F(\cdot)$, as well as the terminal cost $E(\cdot)$, are both of quadratic form, i.e., $F(\hat{\boldsymbol{x}}, \boldsymbol{\tau}) = \hat{\boldsymbol{x}}^\top Q \hat{\boldsymbol{x}} + \boldsymbol{\tau}^\top R \boldsymbol{\tau}$ and $E(\hat{\boldsymbol{x}}) = \hat{\boldsymbol{x}}^\top P \hat{\boldsymbol{x}}$, respectively, with P, Q and R being positive definite matrices. Particularly we define $Q = \text{diag}\{q_1, \ldots, q_8\}$, $R = \text{diag}\{r_1, \ldots, r_4\}$ and $P = \text{diag}\{p_1, \ldots, p_8\}$. Obviously for the running cost function F, we have $F(0,0) = 0$.

Notice, here that the OCP is solved for the nominal system, i.e., the model of the system that is not affected by disturbances. This is the case, due to the fact that the OCP is solved for a prediction horizon, thus, it is not possible to address the disturbances beforehand. However, we distinguish the nominal system that will be denoted as $\hat{\boldsymbol{x}}(\cdot)$ with the actual system, i.e., the system that is affected by disturbances that will be denoted as $\boldsymbol{x}(\cdot)$. Thus, it is shown that the difference between the real evolution of the state, given by (7) and the predicted evolution of the state, given by (5), is in fact, bounded:

Lemma 1: The difference between the actual state $\boldsymbol{x}_{k+j}$ at the time-step $k+j$ and the predicted state $\hat{\boldsymbol{x}}(k+j|k)$ at the same time-step, under the same control sequence, is upper bounded by (See Appendix-I for the Proof):

$$||\boldsymbol{x}_{k+j} - \hat{\boldsymbol{x}}(k+j|k)|| \leq \sum_{i=0}^{j-1} L_f^i \bar{w} \tag{14}$$

Notice that in (11b), the state constraint set X from (8), is being replaced by a restricted constraint set $X_j \subseteq X$. This state constraints' tightening for the nominal system guarantees that the evolution of the real system will be admissible for all time. More specifically, using this technique, it can be guaranteed that the evolution of the state of the perturbed system (7), when the control sequence developed from the NMPC Problem of (11a)-(11d) is applied to it, will necessarily satisfy the state constraint set X. More specifically, given Lemma-1, where a bound on the state prediction error is evaluated, we set $X_j = X \sim \mathscr{B}_j$ where $\mathscr{B}_j = \{\boldsymbol{x} \in \mathbb{R}^8 : ||\boldsymbol{x}|| \leq \sum_{i=0}^{j-1} L_f^i \bar{w}\}$. More details on this constraint tightening technique can be found in [73].

Before proceeding to the necessary robust analysis of the proposed NMPC strategy, we employ some standard stability conditions that are used in MPC frameworks, as the following:

Assumption 1: For the nominal system (5), there is an admissible positively invariant set $\mathscr{E} \subset X$ such that the terminal region $\mathscr{E}_f \subset \mathscr{E}$, where $\mathscr{E} = \{\boldsymbol{x} \in X : ||\boldsymbol{x}|| \leq \varepsilon_0\}$ and ε_0 being a positive parameter.

Assumption 2: We assume that in the terminal set $\mathscr{E}_f$, there exists a local stabilizing controller $\boldsymbol{\tau}_k = h(\boldsymbol{x}_k) \in T$ for all $\boldsymbol{x} \in \mathscr{E}$, and that E satisfies $E(f(\boldsymbol{x}_k, h(\boldsymbol{x}_k))) - E(\boldsymbol{x}_k) + F(\boldsymbol{x}_k, h(\boldsymbol{x}_k)) \leq 0$ for all $\boldsymbol{x} \in \mathscr{E}$.

Assumption 3: The terminal cost function E is Lipschitz in $\mathscr{E}$, with Lipschitz constant $L_E = 2\varepsilon_0\sigma_{max}(P)$ for all $\boldsymbol{x} \in \mathscr{E}$, where $\sigma_{\max}(P)$ denotes the largest singular value of P.

Assumption 4: Inside the set $\mathscr{E}$ we have $E(\boldsymbol{x}) = \boldsymbol{x}^T P \boldsymbol{x} \leq \alpha_\varepsilon$, where $\alpha_\varepsilon = \max\{p_1, \ldots, p_8\}\varepsilon_0^2 > 0$. Assuming that $\mathscr{E}_f = \{\boldsymbol{x} \in X_{(N-1)} : h(\boldsymbol{x}) \in T\}$ and taking a positive parameter α_{ε_f} such that $\alpha_{\varepsilon_f} \in (0, \alpha_\varepsilon)$, we assume that the terminal set designed as $\mathscr{E}_f = \{\boldsymbol{x} \in \mathbb{R}^8 : E(\boldsymbol{x}) \leq \alpha_{\varepsilon_f}\}$ is such that $\forall \boldsymbol{x} \in \mathscr{E},\ f(\boldsymbol{x}, h(\boldsymbol{x})) \in \mathscr{E}_f$.

Lemma 2: The cost function $F(\boldsymbol{x}, \boldsymbol{\tau})$ is such that $F(\mathbf{0}, \mathbf{0}) = 0$ and $\underline{\mathrm{F}}(||\boldsymbol{x}||) \leq F(\boldsymbol{x}, \boldsymbol{\tau}),\ \forall \boldsymbol{x} \in X$and $\forall \boldsymbol{\tau} \in T$ where $\underline{\mathrm{F}}$ is a $\mathcal{K}_\infty$ function. Furthermore, $F(\boldsymbol{x}, \boldsymbol{\tau})$ is Lipschitz continuous with respect to $\boldsymbol{x}$ in X, with a Lipschitz constant $L_F \in \mathbb{R}_{>0}$. Notice that a $\mathcal{K}_\infty$ function, as well as the Lipschitz constant L_F of the Lemma 2, can be found analytically (after some mathematic manipulations), due to the quadratic form of the cost function $F(\boldsymbol{x}, \boldsymbol{\tau})$.

Remark 3 (Thrust's energy consumption): The OCP of the proposed NMPC scheme (11a)-(11d) is designed in order to find the optimal forces $\boldsymbol{\tau}_f^*(\cdot)$ (i.e., minimum forces owing to the quadratic form of the cost function) generated by the thrusters in order to minimize the state error. On the other hand, in (2), we employed a more complete representation of vehicle dynamic equations which incorporate also the ocean currents dynamics. This intuitively means that the OCP of the NMPC is aware of the currents in the region where the vehicle operates, while seeks the minimum forces generated by the thrusters in order to reduce the distance of the robot with respect to the desired position. Thus, owing to the existence of ocean currents profile in the dynamic model (2), the proposed NMPC consequently exploits the ocean current dynamics, if these are in favor of the way point tracking mission. Hence, the proposed control scheme calculates the optimal command inputs, in order to retain the energy consumed by the thrusters in a reduced level, as dictated by the requirements of the considered Problem-1.

Remark 4: The obstacles within the workspace may be detected on–line by the vehicle's on–board sensors (e.g., multi beam imaging or side scan sonar). In such a case, it should be assured that the predicted state of the NMPC is always within the sensing region of the robot. This intuitively means that the prediction state is always feasible even in the worst case (i.e., maximum velocity of the robot under maximum sea current). Thus, assuming that $\bar{R}$ denotes the sensing range of the system, the prediction horizon N should be set as follows:

$$N \leq \frac{\bar{R}}{(|\bar{\boldsymbol{v}}_1| + |\bar{\boldsymbol{v}}_c|)dt}$$

where the $|\bar{\boldsymbol{v}}_1|$ is the norm of maximum linear velocity of the vehicle and $|\bar{\boldsymbol{v}}_c|$ is the norm of the upper bound of the sea current velocity.

E. Stability Analysis of the Proposed NMPC

The approach for establishing stability consists of two parts: in the first part it is shown that the initial feasibility implies feasibility afterwards and based on this, it is then shown that the state converges to a bounded set, due to the presence of the persistent disturbances [73]–[76]. We begin by denoting $\boldsymbol{\tau}_f^*(k-1)$ as the optimal solution that results from (11a)-(11d) at a time-step $k-1$. We, also, denote a feasible control sequence $\tilde{\boldsymbol{\tau}}_f(k+j|k)$ of the optimization problem at time-step k, such as:

$$\tilde{\boldsymbol{\tau}}(k+j|k) = \begin{cases} \boldsymbol{\tau}^*(k+j|k-1) & \text{for } j = 0, \ldots, N-2 \\ h(\hat{\boldsymbol{x}}(k+N-1|k)) & \text{for } j = N-1 \end{cases} \tag{15}$$

where $h(\boldsymbol{x})$ is the local stabilizing controller defined in *Assumption 2*. Moreover, from (11c) and *Assumption 2* is clear that $\tilde{\boldsymbol{\tau}}(k+j|k) \in T$.

Feasibility analysis:

First we are going to provide a necessary definition: Let $\mathcal{X}^{MPC}$ be the set containing all the state vectors for which a feasible control sequence exists that satisfies the constraints of the optimal control problem. In particular, while having a slight violation of the notation we can define the feasible set $\mathcal{X}^{MPC}$ as follows:

Definition 1: $\mathcal{X}^{MPC} = \{\boldsymbol{x}_0 \in \mathbb{R}^n | \exists$ a control sequence $\boldsymbol{\tau}_f \in T,\ \hat{\boldsymbol{x}}_f(j) \in \mathcal{X}_j\ \ \forall j \in \{1, \ldots, N\}$ and $\hat{\boldsymbol{x}}(N) \in \mathcal{E}_f\}$.

At this point we want to find a bound $\bar{w}$ for the uncertainties, then the closed-loop system in $\mathcal{X}^{MPC}$ is stable. That means that if $\boldsymbol{x}_k \in \mathcal{X}^{MPC}$ then $\boldsymbol{x}_{k+1} = f(\boldsymbol{x}_k, \boldsymbol{\tau}_k^*) + \boldsymbol{w}_{k+1} \in \mathcal{X}^{MPC}$, for all $\boldsymbol{w}_{k+1} \in W$. In order to derive feasibility it must be guaranteed that $\hat{\boldsymbol{x}}(k+N|k) \in \mathscr{E}_f$. This results to a permitted upper bound of disturbances $\bar{w}$ under which the system is proven to be feasible. See Appendix-II for the Proof.

Convergence analysis:

In order to treat the convergence property, it should be guaranteed that the state of the perturbed system reaches to a desired terminal set. A proper value function must be shown to be decreasing in order to prove stability of the closed loop system and consequently the state convergence of the system. Consider the optimal cost $J_N^*(k-1) = J^*(\boldsymbol{x}_{k-1}, \boldsymbol{\tau}_f^*(k-1))$ from (11a), at the time-step $(k-1)$ as a Lyapunov function candidate. Consider, also, the cost of the feasible sequence at time-step k as $\tilde{J}_N(k) = \tilde{J}(\boldsymbol{x}_k, \tilde{\boldsymbol{\tau}}_f(k))$ evaluated from the control sequence $\tilde{\boldsymbol{\tau}}_f(k+i|k)$. After some mathematical manipulations, it can be hold for the difference $\tilde{J}_N(k) - J_N^*(k-1)$ that (See Appendix-III for the Proof):

$$\begin{aligned} \Delta J = \tilde{J}_N(k) - J_N^*(k-1) &\leq \left(L_F \sum_{i=0}^{i=N-2} L_f^i + L_E L_f^{N-1} \right) \bar{w} \\ &- F(\hat{\boldsymbol{x}}(k-1|k-1), \boldsymbol{\tau}^*(k-1|k-1)) \\ &\leq \left(L_F \sum_{i=0}^{i=N-2} L_f^i + L_E L_f^{N-1} \right) \bar{w} - \underline{\mathrm{F}}(||\boldsymbol{x}_{k-1}||) \end{aligned}$$

From the optimality of the solution, we derive the following:

$$\Delta J^* = J_N^*(k) - J_N^*(k-1) \leq \Delta J \tag{16}$$

Therefore, the optimal cost $J_N^*(k)$ is an ISS-Lyapunov function of the closed loop system, and hence, the closed-loop system is input-to-state stable.

IV. EXPERIMENTAL RESULTS

This section demonstrates the efficacy of the proposed motion control scheme via a set of real-time experiments

employing a small underwater robotic vehicle. In particular, Subsection IV-A introduces the experimental setup and Subsection IV-B presents the detailed results of two cases of experimental studies with the proposed controller.

A. Experimental Setup

The experiments were carried out inside the *NTUA, Control Systems Lab* test tank, with dimensions $5m \times 3m \times 1.5m$ (Fig. 4). The bottom of the tank is covered by a custom-made poster with various visual features and markers. Two cylindrical objects with known position and dimensions are placed inside the tank and considered as static obstacles. The vehicle used

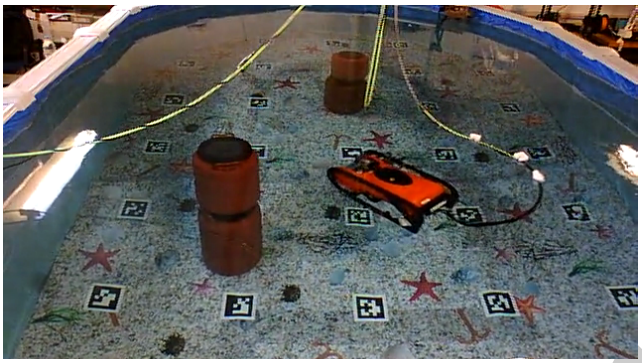

Fig. 4: Experimental setup: The 4 DoFs Seabotix LBV inside of the NTUA, Control Systems Lab test tank including obstacles.

in this work is a 4 DoFs Seabotix LBV, actuated in Surge, Sway, Heave and Yaw via a 4 thruster set configuration as depicted in Fig. 5. Thus, the thrust allocator matrix $\boldsymbol{T_A}$ of eq. (3) is calculated and given as[2]:

$$\boldsymbol{T_A} = \begin{bmatrix} 1 & 1 & 0 & 0 \\ 0 & 0 & 0 & 1 \\ 0 & 0 & 1 & 0 \\ 0.0475 & -0.0475 & 0 & 0.05 \end{bmatrix}$$

The vehicle is equipped with a down-looking Sony PlayStation Eye camera, with 640×480 pixels at 30 frames per second (fps) enclosed in a waterproof housing. An underwater laser pointer projecting a green dot at the bottom of the test tank is rigidly attached on the vehicle with its axes aligned to the down-looking camera axis. The vehicle is also equipped with an $SBG\ IG-500A$ AHRS, delivering temperature-compensated 3D acceleration, angular velocity and orientation measurements at $100Hz$. The marker localization system is based on the $ArUco$ library [78]. The complete state vector of the vehicle ($3D$ position, orientation, velocity) as well as the vehicle's dynamic parameters in the following experimental studies are available via the sensor fusion and state estimation module based on the Complementary Filter notion and a proper identification scheme presented in our previous results [77]. The identified dynamic parameters of the vehicle are given in Table-I. The analysis of the sensor fusion, state estimation and parameter identification algorithms are out of

[2]More details about calculation of the thrust allocator matrix can be found in [77]

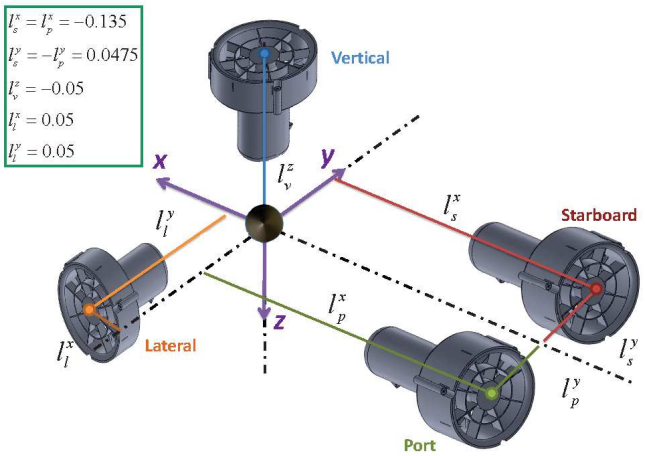

Fig. 5: The LBV150 thruster configuration.

the scope of this work and thus omitted. However, they can be found in detail in [77] . The software implementation of the proposed motion control scheme was conducted in C++ and Python under the Robot Operating System (ROS) [79]. Moreover, the Nonlinear Model Predictive Controller employed in this work is designed using the NLopt Optimization library [80] and runs on a desktop with 8 cores, 3.60 GHz CPU and 16 GB of RAM at $10Hz$. Furthermore, various controller parameters for all of the following experiments are presented in Table-II. The disturbances in the form of water currents,

TABLE I: Vehicle identified dynamic parameter set

m_{11}	m_{22}	m_{33}	m_{44}
9.7532	8.6636	10.898	0.1589
X_u	Y_v	Z_w	N_r
-8.6040	-18.1106	-17.1828	-1.4146
$X_{\|u\|u}$	$Y_{\|v\|v}$	$Z_{\|w\|w}$	$N_{\|r\|r}$
-17.8534	-1.0594	-3.6482	-10.3483

were induced using a $BTD150$ thruster properly mounted inside the water tank. The generated flow field (i.e., assumed ocean current profile), was computed using a GPU-enabled Computational fluid Dynamics (CFD) software [81] developed in the Parallel CFD and Optimization Unit of the school of Mechanical Engineering of NTUA. The flow field distribution inside the water tank is depicted in Fig-6.

TABLE II: MPC parameters

Parameter	Value
Prediction horizon N	6
Lipschitz constant[3] L_f	1.1
positive constant[4] ε_0	0.541
Cost function matrices	$P = Q = \text{diag}\{5\}$, $R = \text{diag}\{1.5\}$
Uncertainties upper bound $\bar{w}$	0.15
Lipschitz constant L_E	$L_E = 2\varepsilon_0\sigma_{max}(P) = 5.41$
constant α_ε	$\alpha_\varepsilon = \max\{p_1, \ldots, p_8\}\varepsilon_0^2 = 1.4634$
constant α_{ε_f}	0.1

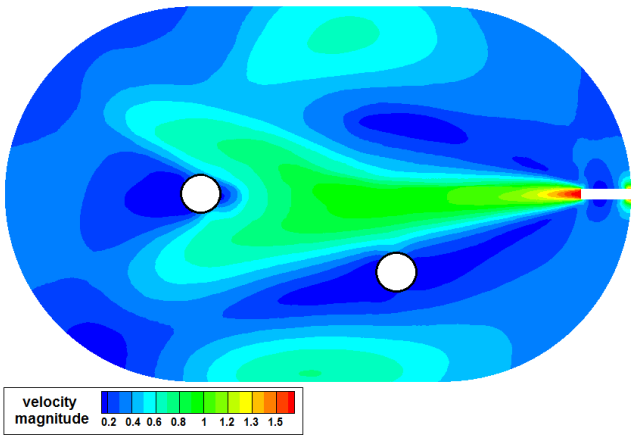

Fig. 6: Distribution of the flow field inside the experimental water tank as computed by the CFD software presented in [81].

B. Results

In order to prove the efficiency of the proposed controller, three experimental sessions are presented, namely Session A, B and C. In all experiments the objective is to follow a set of predefined way points, while simultaneously avoid two static obstacles and respect the workspace (test tank) boundaries. In Sessions A and B, we consider the dynamic model of vehicle in which the ocean currents are incorporated, hence the controller is aware about the presence of currents. In Sessions A and B, two different experiments were conducted for each case, namely A.1, A.2, B.1, B.2, demonstrating in this way the repeatability of the proposed control strategy. In Session C, the employed dynamic model of vehicle inside the OPC of NMPC, is not aware of the water currents induced by the thruster mounted inside the water tank. A comparative study is then presented, describing the performance of the underwater robot along with the consumed thrust, in both cases where the currents are known and unknown. The location and geometry of the obstacles are considered known. More specific, the position of the obstacles w.r.t the Inertial Frame $\mathcal{I}$ in $x-y$ plane is given by: $x_{obs_1} = \begin{bmatrix} -0.625 & -0.625 \end{bmatrix}$, $x_{obs_2} = \begin{bmatrix} 0.9375 & 0 \end{bmatrix}$. Moreover, their length is considered to reach above the water surface in order to prevent the MPC algorithm from calculating solutions that impose the vehicle to bypass them over the top. The state constraints of the (9a)-(9d) which must be satisfied during all the experiments are analytically formulated as follows: i) The obstacles are cylinders (See Fig.4) with radius $r_{\pi_i} = 0.16m,\ i = \{1, 2\}$ and are modeled together with the workspace boundaries according to the spherical world representations as consecutive spheres. ii) The radius of the sphere $\mathcal{B}(\boldsymbol{\eta}_1, \bar{r})$ which covers all the vehicle volume (i.e., main body and additional equipment) is defined as $\bar{r} = 0.3m$. However, for the clarity of presentation, we depict it as a safe zone around the obstacles where the vehicle center $\boldsymbol{\eta}_1$ (denoted by blue line, see Fig.7, Fig.12, Fig.17) should not violated it. iii) The vertical position must be between $0 < z < 1.2\ m$. iv) The vehicle's body velocity norm of (9a) $|u_r + v_r|$ (planar motion) must not exceed $0.5m/s$. v) Heave velocity must be retained between $-0.25 < w_r < 0.25\ m/s$ (i.e., $0.25 - |w_r| \geq 0$). vi) Yaw velocity must be retained between $-1 < r_r < 1\ rad/s$ (i.e., $1 - |r_r| \geq 0$). Moreover, each of the four thrusters must obey the following input constraint: $-12 < \tau_i < 12N,\ i = \{p,\ s,\ v,\ l\}$. The state and input constraints in the following figures are depicted in red dashed lines were applicable. At this point we should mention that each mission is considered as successful only if the vehicle performs the way point tracking three consecutive times, hence repeatability is proved. In all times the vehicle is under the influence of the water currents depicted in Fig 6.

[3]The calculation of the smallest Lipschitz constant for a robotic system is out of scope of this work and thus omitted.

[4]In all of the following experiments, the vehicle is consider to reach each way point if it has entered a terminal region (i.e., spherical region with radius $0.3m$ and a offset of $\pm 0.15rad$) around the way point.

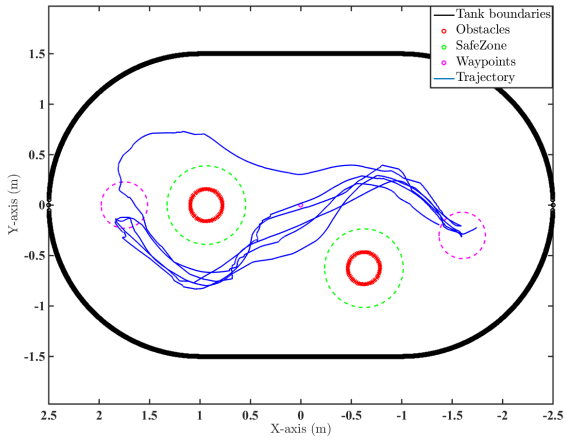

(a) A.1 experiment

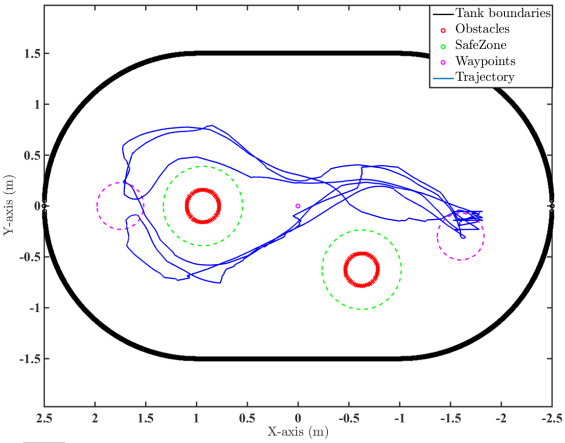

(b) A.2 experiment

Fig. 7: Session A – 2 WP tracking scenario: Vehicle trajectory in horizontal plane

*1) **Session A – Two Way Points Tracking**:* In this scenario the vehicle must travel via two way points which are placed at $\boldsymbol{\eta}_1^d = \begin{bmatrix} -1.60\,m & -0.35\,m & 0.45\,m & 0\,rad \end{bmatrix}$, $\boldsymbol{\eta}_2^d = \begin{bmatrix} 1.75\,m & 0\,m & 0.30\,m & \pi\,rad \end{bmatrix}$ respectively. The three consecutive trajectories of the vehicle along the horizontal plane are depicted in Fig. 7 for each of the two experiments. It can be seen that the vehicle performs successfully the way point tracking while safely avoids the obstacles and the test tank boundaries. We observe that in some cases the vehicle may travel from one way point to the other following a

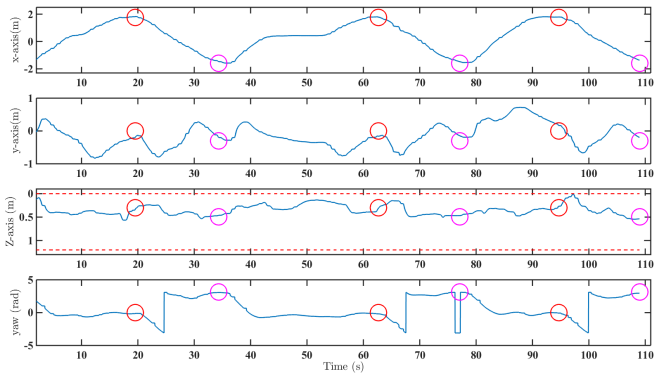

(a) A.1 experiment

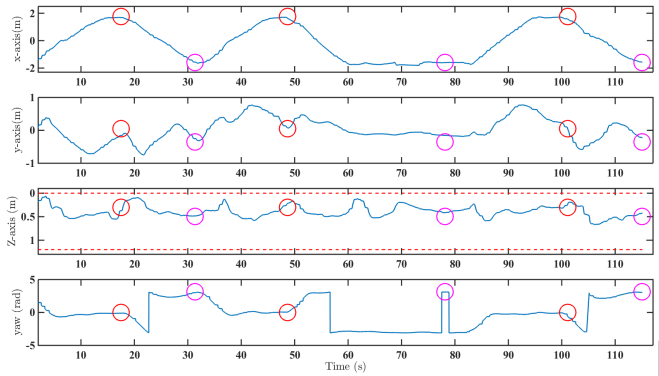

(b) A.2 experiment

Fig. 8: Session A – 2 WP tracking scenario: Evolution of vehicle states

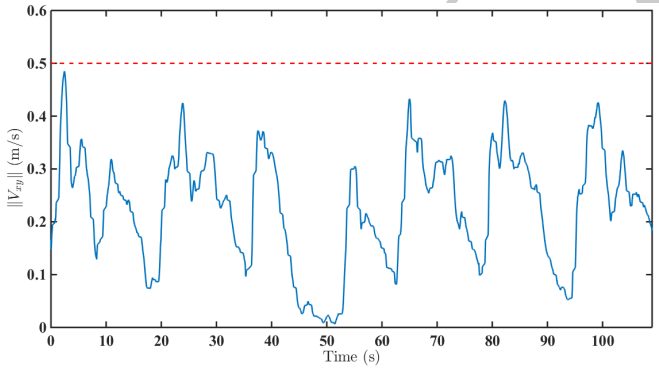

(a) A.1 experiment

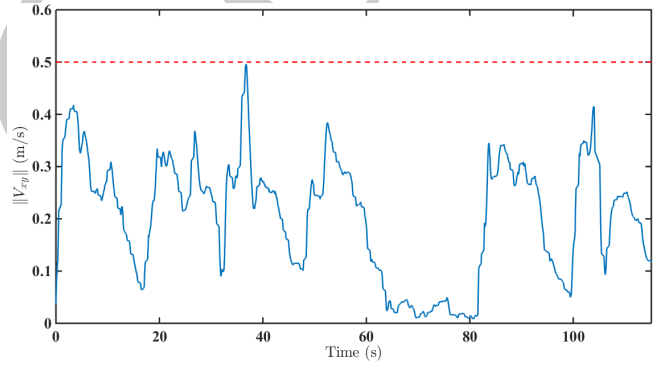

(b) A.2 experiment

Fig. 9: Session A – 2 WP tracking scenario: Vehicle body velocity norm $|u_r + v_r|$

different trajectory. This can be explained by the fact that the MPC finds a different optimal solution at the specific time frame, due to the unmodeled dynamics of the tether which significantly affect the vehicle motion. The vertical and angular motion of the vehicle are depicted in Fig. 8, where it can be seen that the state constraints are always satisfied. The vehicle is consider to reach each way point if it has entered a terminal region (i.e., spherical region of $0.3m$ and a offset of $\pm 0.15rad$) around the way point. These regions are depicted in circles in Fig. 7 and 8. In Fig. 9 the body velocity norm in planar motion is depicted and the respective constraint is satisfied. The same stands for the heave and yaw velocities, as shown in Fig. 10. In Fig. 11 the vehicle's thruster inputs are shown. As it can be seen the input constraints are also satisfied.

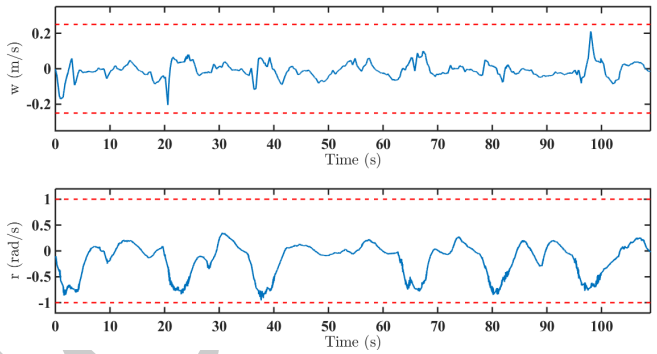

(a) A.1 experiment

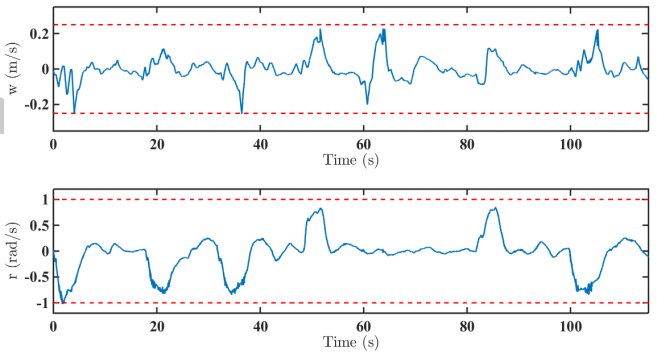

(b) A.2 experiment

Fig. 10: Session A–2 WP tracking scenario: Vehicle heave and yaw velocities

*2) **Session B – Three Way Points Tracking**:* This scenario is similar to the previous one except that the vehicle must travel along 3 way points which makes the mission more challenging considering the narrow workspace. The locations of the three way points are given by: $\boldsymbol{\eta}_1^d = \left[-1.50\,m, 0.30\,m, 0.40\,m, -\frac{\pi}{2}\,rad\right]$, $\boldsymbol{\eta}_2^d = [0.45\,m, -1\,m, 0.25\,m, 0\,rad]$, $\boldsymbol{\eta}_3^d = [1.20\,m,\ 1\,m, 0.30\,m, -\pi\,rad]$. Again for this scenario, two experiments were carried out. The three consecutive trajectories of the vehicle along the horizontal plane are depicted in Fig. 12. Although this scenario is more complicated, the vehicle again carries it out successfully. In this mission, the vehicle also follows different trajectories, for the same reasons explained in Session A. The vertical and angular motion are depicted in Fig. 13, while in Fig. 14 the

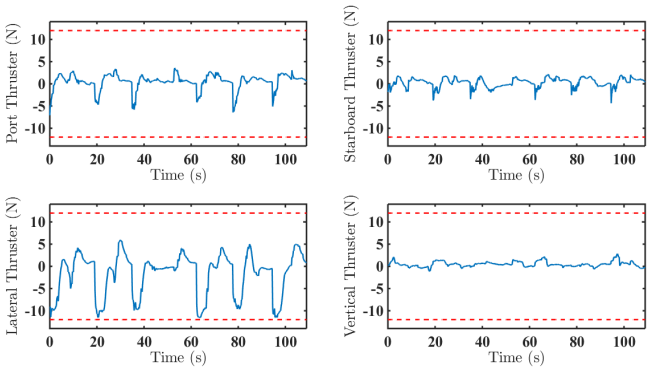

(a) A.1 experiment

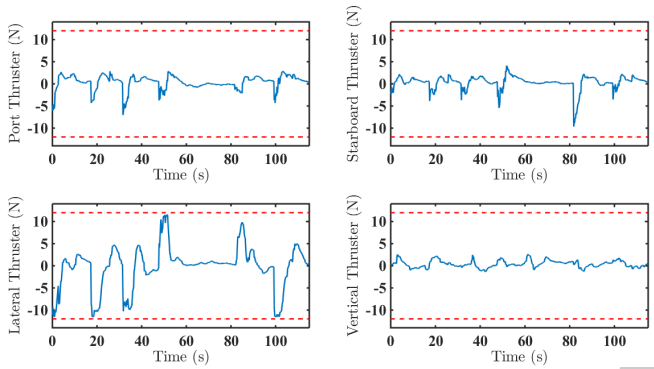

(b) A.2 experiment

Fig. 11: Session A – 2 WP tracking scenario: Thruster Commands

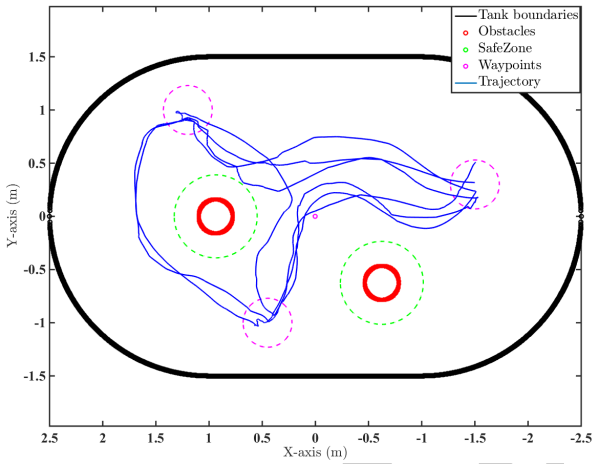

(a) B.1 experiment

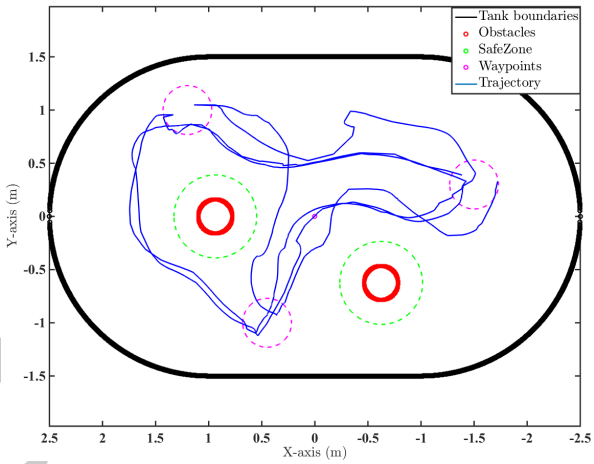

(b) B.2 experiment

Fig. 12: Session B – 3 WP tracking scenario: Vehicle trajectory in horizontal plane

body velocity norm in planar motion is shown. The heave and yaw velocities are presented in Fig. 15, while in Fig. 16 the vehicle's thruster inputs are shown. As it can be observed, the vehicle reached all desired way points while simultaneously satisfied all respective state and input constraints.

*3) **Session C – Comparative Experimental Results**:* In the following experiment, the vehicle must travel again along 3 way points, which is considered as the more challenging case. The location of the three way points is exactly the same as in Session B. However, the predictive controller considers the dynamic model of the vehicle in which the ocean currents are not incorporated. Hence, the employed dynamic model inside the OCP of the NMPC is not aware of the water currents induced by the thruster mounted inside the water tank. More precisely, instead of Eq. (2), we employ the simple dynamic model, as given in [71, eq:2.172-2.173]:

$$\dot{\boldsymbol{\eta}} = \boldsymbol{J}(\boldsymbol{\eta})\,\boldsymbol{v} \tag{17a}$$

$$\boldsymbol{M}\dot{\boldsymbol{v}} + \boldsymbol{C}(\boldsymbol{v})\,\boldsymbol{v} + \boldsymbol{D}(\boldsymbol{v})\boldsymbol{v} + \boldsymbol{g}(\boldsymbol{\eta}) = \boldsymbol{\tau}_{\mathcal{V}} \tag{17b}$$

The three consecutive trajectories of the vehicle along the horizontal plane are depicted in Fig.17. It can be seen that the vehicle follows different trajectories each time. In addition to the reasons explained in Session A, the water currents act as unmodeled and dynamic external disturbances. Comparing Fig.17 with Fig. 12, and taking into account the distribution of the flow field inside the water tank, as indicated in Fig.6, it can be observed that in the first case (Fig. 12) the robot has exploited the known water current dynamics during its way point tracking mission. On the contrary, when the water currents were not known to the system (Fig. 17), in one of the three consecutive trajectories, the vehicle traveled outside the area between the obstacles and close to the water tank boundary, while moving between the first way point to the second one. In Fig.18 the body velocity norm in planar motion is shown, where it can be observed that the predefined velocity constraint has been violated at least once.

The vehicle's thruster inputs are shown in Fig. 19. A comparison between the thrust consumption in Sessions B (known current profile) and C (unknown current profile) is given in Tables III-IV. It is shown that the consumed thrust in B.1 and B.2 experiments is significant less relative to Session C experiment. It is also worth noticing that B.2 experiment was completed in only $128.5\ sec$ while the Session C experiment lasted $161.8\ sec$. We can also observe, that while B.1 experiment had almost the same time duration with C (i.e., $160.1\ sec$), a significant 15% reduction on the thrust consumption occurred. Hence, the proposed control scheme appears to be more efficient and optimal in terms of thrust consumption. According to Table IV, no significant difference in thrust consumption appears in the vertical direction. This is explained by the fact, that (for the sake of simplicity) we

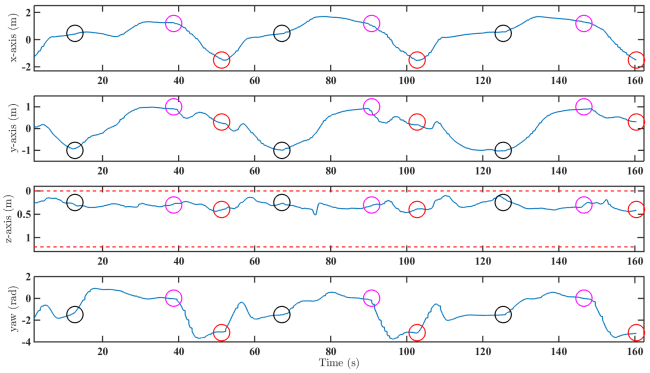

(a) B.1 experiment

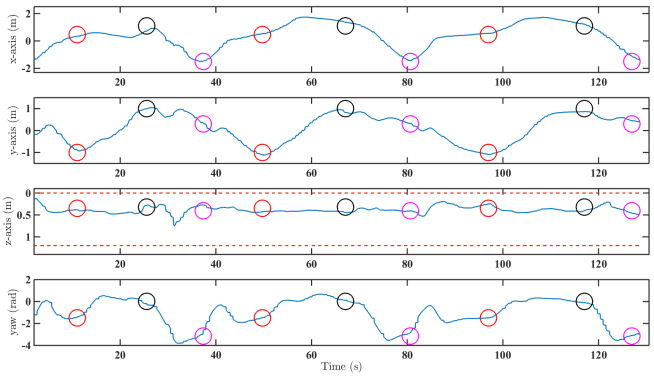

(b) B.2 experiment

Fig. 13: Session B – 3 WP tracking scenario: Evolution of vehicle states

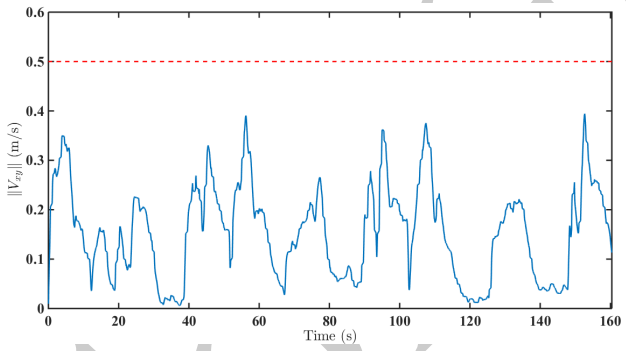

(a) B.1 experiment

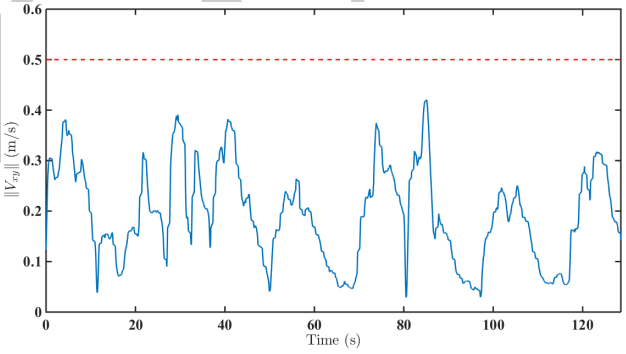

(b) B.2 experiment

Fig. 14: Session B – 3 WP tracking scenario: Vehicle body velocity norm $|u_r + v_r|$

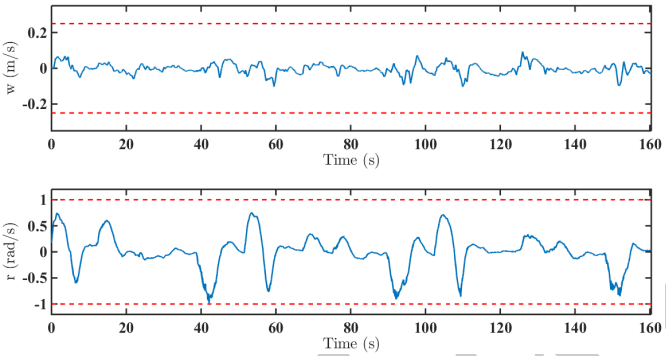

(a) B.1 experiment

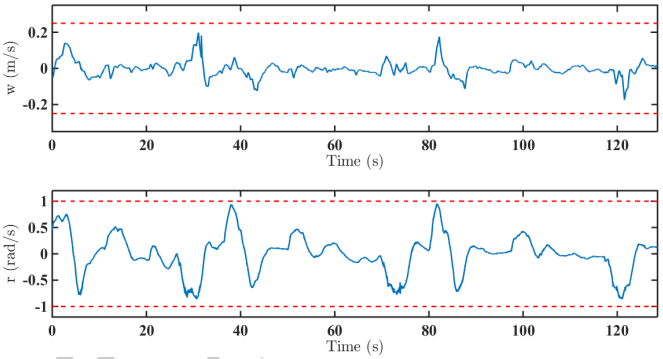

(b) B.2 experiment

Fig. 15: Session B – 3 WP tracking scenario: Vehicle heave and yaw velocities

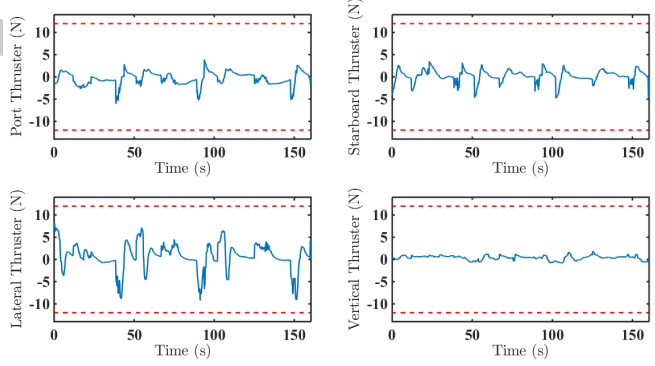

(a) B.1 experiment

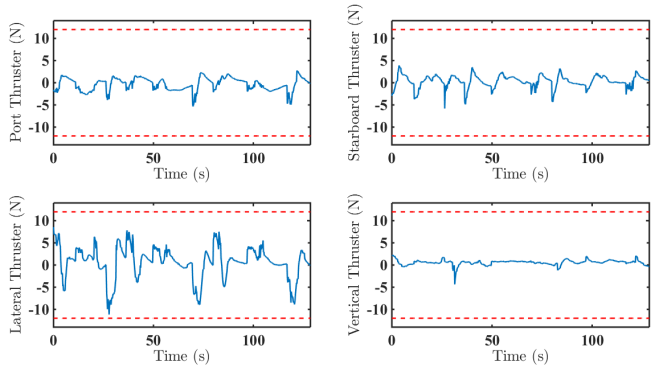

(b) B.2 experiment

Fig. 16: Session B – 3 WP tracking scenario: Thruster Commands

considered a $2D$ (i.e., in horizontal plane) distribution of the flow field inside the water tank and accordingly was computed the flow by the CFD software [81]. However, it is expected that more convincing results can be achieved if a more realistic model of the water current (i.e., $3D$ space) is employed within the dynamic model of the proposed predictive controller.

TABLE III: Thrust consumption comparison

Thruster	Thrust absolute value (N)		
	B.1 Exp	B.2 Exp	C Exp
Port	1161.5	946.7	1329.5
Starboard	954.0	846.4	1328.7
Lateral	1957.0	1942.5	2249.2
Vertical	940.3	925.5	1001.8
Total	5012.8	4661.1	5909.2
Total Reduction w.r.t C Exp	-15%	-21%	

TABLE IV: Exploitation per thruster

Thruster	Thrust Reduction w.r.t to Session C Experiment	
	B.1 Exp	B.2 Exp
Port	-12.6%	-28.8%
Starboard	-28.2%	-36.3%
Lateral	-12.9%	-13.6%
Vertical	-6.1%	-7.6%

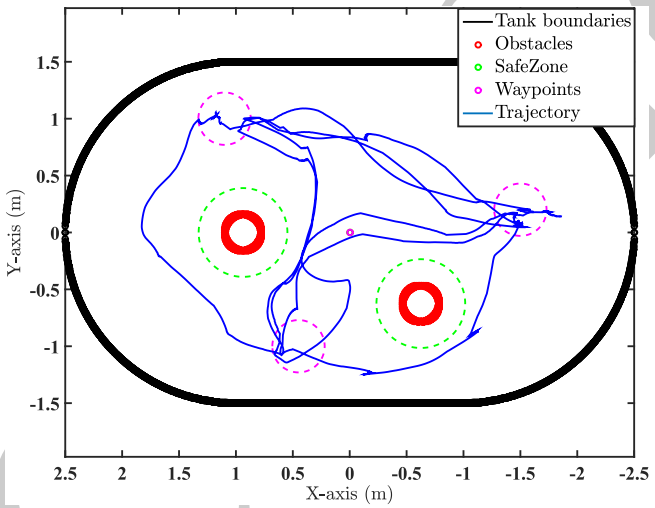

Fig. 17: Session C – Comparative scenario: Vehicle trajectory in horizontal plane

VIDEO

A video demonstrating the aforementioned experimental results of the proposed methodology can be found at the following url: https://youtu.be/z04ELMfCTYk

V. CONCLUSION

In this paper, we presented a novel Model predictive Control strategy for underwater robotic vehicles operating in a constrained workspace including obstacles. The purpose of this control scheme is to guide the vehicle towards specific way points. Various constraints such as: obstacles, workspace boundaries, thruster saturation and predefined upper bound of the vehicle velocity (requirements for various underwater tasks such as seabed inspection, mosaicking etc.) are considered during the control design. Moreover, the proposed control scheme incorporates the dynamics of the vehicle and is designed in order to find optimal thrusts required for minimizing the way point tracking error. The control inputs calculated by the proposed scheme, may exploit the ocean currents when these are in favor of the way point tracking mission, which results in retaining the energy consumed by the thrusters in a reduced level. The efficacy of the proposed controller is experimentally verified using a 4 Degrees of Freedom (DoF) underwater robotic vehicle inside a constrained test tank with sparse static obstacles. Future research efforts will be devoted towards extending the proposed methodology for multiple underwater vehicles operating in a dynamic environment including not only static but also moving obstacles.

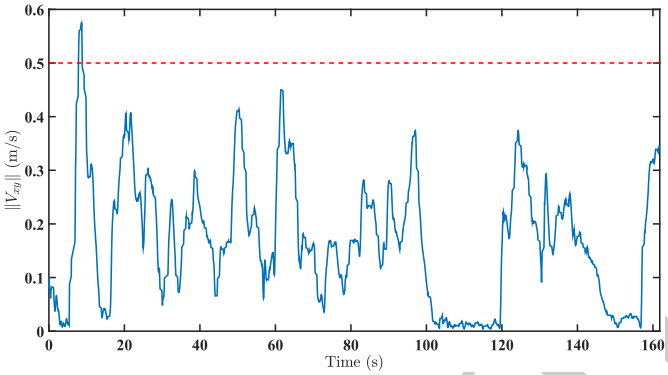

Fig. 18: Session C – Comparative scenario: Vehicle body velocity norm $|u_r + v_r|$

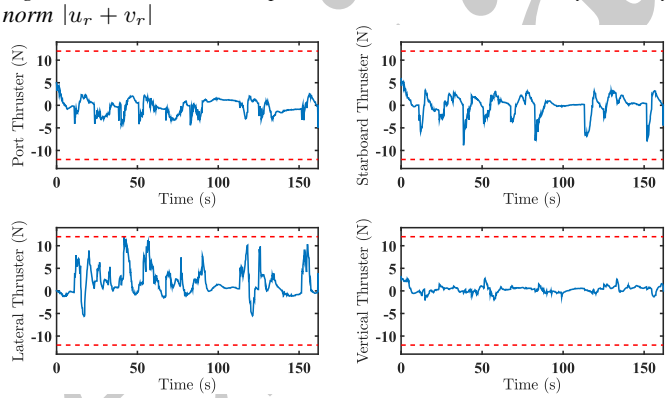

Fig. 19: Session C – Comparative scenario: Thruster Commands

VI. APPENDICES

APPENDIX I

In view of the Property-1 and using triangle inequality we get:

$$||\boldsymbol{x}_{k+1} - \hat{\boldsymbol{x}}(k+1|k)|| =$$
$$||f(\boldsymbol{x}_k, \boldsymbol{\tau}_k) + \boldsymbol{w}_k - f(\hat{\boldsymbol{x}}(k|k), \boldsymbol{\tau}_k)|| = ||\boldsymbol{w}_k|| \leq \bar{w}$$
$$||\boldsymbol{x}_{k+2} - \hat{\boldsymbol{x}}(k+2|k)|| =$$
$$||f(\boldsymbol{x}_{k+1}, \boldsymbol{\tau}_{k+1}) + \boldsymbol{w}_{k+1} - f(\hat{\boldsymbol{x}}(k+1|k), \boldsymbol{\tau}_{k+1})||$$

$$\leq ||f(\boldsymbol{x}_{k+1}, \boldsymbol{\tau}_{k+1}) - f(\hat{\boldsymbol{x}}(k+1|k), \boldsymbol{\tau}_{k+1})|| + ||\boldsymbol{w}_{k+1}||$$
$$\leq L_f||\boldsymbol{x}_{k+1} - \hat{\boldsymbol{x}}(k+1|k)|| + ||\boldsymbol{w}_{k+1}|| \leq (1+L_f)\bar{w}$$
$$\vdots$$
$$||\boldsymbol{x}_{k+j} - \hat{\boldsymbol{x}}(k+j|k)|| \leq \sum_{i=0}^{j-1}(L_f)^i\bar{w}$$

APPENDIX II

In order to prove this, first it will be shown that:

$$||\hat{\boldsymbol{x}}(k|k) - \hat{\boldsymbol{x}}(k|k-1)|| = \boldsymbol{w}_k \leq \bar{w}$$
$$||\hat{\boldsymbol{x}}(k+1|k) - \hat{\boldsymbol{x}}(k+1|k-1)|| =$$
$$= ||f(\hat{\boldsymbol{x}}(k|k)) - f(\hat{\boldsymbol{x}}(k|k-1))||$$
$$\leq L_f(||\hat{\boldsymbol{x}}(k|k) - \hat{\boldsymbol{x}}(k|k-1)||) \leq L_f \cdot \bar{w}$$
$$\vdots$$
$$||\hat{\boldsymbol{x}}(k+N-1|k) - \hat{\boldsymbol{x}}(k+N-1|k-1)|| \leq L_f^{N-1} \cdot \bar{w}$$

From *Assumption 3* we have:

$$E(\hat{\boldsymbol{x}}(k+N-1|k)) - E(\hat{\boldsymbol{x}}(k+N-1|k-1)) \leq$$
$$\leq L_E||\hat{\boldsymbol{x}}(k+N-1|k) - \hat{\boldsymbol{x}}(k+N-1|k-1)|| \leq L_E \cdot L_f^{N-1} \cdot \bar{w}$$

For the nominal system and based on the optimal solution $\boldsymbol{\tau}^*(k+j|k-1)$ we have: $\hat{\boldsymbol{x}}(k+N-1|k-1) \in \mathscr{E}_f$. Therefore, taking into account *Assumption 4*:

$$E(\hat{\boldsymbol{x}}(k+N-1|k)) \leq \alpha_{\varepsilon_f} + L_E \cdot L_f^{N-1} \cdot \bar{w}$$

we want $\hat{\boldsymbol{x}}(k+N-1|k)$ to belong to the set $\mathscr{E}$, thus from *Assumption 4* it must satisfy $E(\hat{\boldsymbol{x}}(k+N-1|k)) \leq \alpha_\varepsilon$, which leads to:

$$E(\hat{\boldsymbol{x}}(k+N-1|k)) \leq \alpha_{\varepsilon_f} + L_E \cdot C_f^{N-1} \cdot \bar{w} \leq \alpha_\varepsilon$$

Therefore, if the uncertainties of the system are bounded by $\bar{w} \leq \frac{\alpha_\varepsilon - \alpha_{\varepsilon_f}}{L_E \cdot L_f^{N-1}}$ then $\hat{\boldsymbol{x}}(k+N-1|k)$ belongs to the set $\mathscr{E}$, and from *Assumption 4* we get $\hat{\boldsymbol{x}}(k+N|k) \in \mathscr{E}_f$.

APPENDIX III

The difference between the optimal cost and the feasible cost is:

$$\Delta J = \tilde{J}_N(k) - J_N^*(k-1) =$$
$$= \sum_{i=0}^{i=N-1} F(\tilde{\boldsymbol{x}}(k+i|k), \tilde{\boldsymbol{\tau}}(k+i|k)) + E(\tilde{\boldsymbol{x}}(k+N|k))$$
$$- \sum_{i=0}^{i=N-1} F(\hat{\boldsymbol{x}}(k+i-1|k-1), \boldsymbol{\tau}^*(k+i-1|k-1))$$
$$- E(\hat{\boldsymbol{x}}(k+N-1|k-1)) = \sum_{i=0}^{i=N-2} F(\tilde{\boldsymbol{x}}(k+i|k), \tilde{\boldsymbol{\tau}}(k+i|k))$$
$$- F(\hat{\boldsymbol{x}}(k+i|k-1), \boldsymbol{\tau}^*(k+i|k-1))$$
$$+ F(\tilde{\boldsymbol{x}}(k+N-1|k), \tilde{\boldsymbol{\tau}}(k+N-1|k))$$
$$- F(\hat{\boldsymbol{x}}(k-1|k-1), \boldsymbol{\tau}^*(k-1|k-1))$$
$$+ E(\tilde{\boldsymbol{x}}(k+N|k)) - E(\hat{\boldsymbol{x}}(k+N-1|k-1))$$

where $\tilde{\boldsymbol{\tau}}(k+N-1|k) = h(\hat{\boldsymbol{x}}(k+N-1|k))$ taken from (15) and $\tilde{\boldsymbol{\tau}}(k+i|k) = \boldsymbol{\tau}^*(k+i|k-1)$ for $i = 0, \ldots, N-2$. Also from *Lemma 2* combined with *Lemma 1* we get:

$$\sum_{i=0}^{i=N-2} F(\tilde{\boldsymbol{x}}(k+i|k), \tilde{\boldsymbol{\tau}}(k+i|k))$$
$$- F(\hat{\boldsymbol{x}}(k+i|k-1), \boldsymbol{\tau}^*(k+i|k-1))$$
$$\leq L_F \cdot \sum_{i=0}^{i=N-2} L_f^i \cdot \bar{w}$$

From *Assumption 3* it yields:

$$E(\tilde{\boldsymbol{x}}(k+N|k)) - E(\hat{\boldsymbol{x}}(k+N-1|k-1))$$
$$= E(\tilde{\boldsymbol{x}}(k+N|k)) - E(\tilde{\boldsymbol{x}}(k+N-1|k))$$
$$+ E(\tilde{\boldsymbol{x}}(k+N-1|k)) - E(\hat{\boldsymbol{x}}(k+N-1|k-1))$$
$$\leq E(\tilde{\boldsymbol{x}}(k+N|k)) - E(\tilde{\boldsymbol{x}}(k+N-1|k)) + L_E L_f^{N-1}\bar{w}$$

We used the instantaneous difference of the predictive state $\hat{\boldsymbol{x}}(k+N-1|k)$ and the feasible state $\tilde{\boldsymbol{x}}(k+N-1|k-1)$ at the time-step $k+N-1$ such that:

$$||\tilde{\boldsymbol{x}}(k+N-1|k-1) - \hat{\boldsymbol{x}}(k+N-1|k)|| \leq L_f^{N-1}\bar{w}$$

Therefore, we obtain:

$$\Delta J \leq \left(L_F \sum_{i=0}^{i=N-2} L_f^i + L_E L_f^{N-1}\right)\bar{w} +$$
$$+ \Big[F(\tilde{\boldsymbol{x}}(k+N-1|k), h(\hat{\boldsymbol{x}}(k+N-1|k)))$$
$$+ E(\tilde{\boldsymbol{x}}(k+N|k)) - E(\tilde{\boldsymbol{x}}(k+N-1|k))\Big]$$
$$- F(\hat{\boldsymbol{x}}(k-1|k-1), \boldsymbol{\tau}^*(k-1|k-1))$$

Finally, taking into account the *Assumption 2* and *Lemma2*:

$$\Delta J \leq \left(L_F \sum_{i=0}^{i=N-2} L_f^i + L_E L_f^{N-1}\right)\bar{w} -$$
$$- F(\hat{\boldsymbol{x}}(k-1|k-1), \boldsymbol{\tau}^*(k-1|k-1))$$
$$\leq \left(L_F \sum_{i=0}^{i=N-2} L_f^i + L_E L_f^{N-1}\right)\bar{w} - \underline{\mathrm{F}}(||\boldsymbol{x}_{k-1}||)$$

REFERENCES

[1] J. Yuh, "Design and control of autonomous underwater robots: A survey," *Autonomous Robots*, vol. 8, no. 1, pp. 7–24, 2000.

[2] Z. Zeng, L. Lian, K. Sammut, F. He, Y. Tang, and A. Lammas, "A survey on path planning for persistent autonomy of autonomous underwater vehicles," *Ocean Engineering*, vol. 110, pp. 303–313, 2015.

[3] O. Hasvold, N. Størkersen, S. Forseth, and T. Lian, "Power sources for autonomous underwater vehicles," *Journal of Power Sources*, vol. 162, no. 2 SPEC. ISS., pp. 935–942, 2006.

[4] T. Joung, K. Sammut, F. He, and S.-K. Lee, "A study on the design optimization of an auv by using computational fluid dynamic analysis," *Proceedings of the International Offshore and Polar Engineering Conference*, pp. 696–702, 2009.

[5] D. N. Subramani and P. F. Lermusiaux, "Energy-optimal path planning by stochastic dynamically orthogonal level-set optimization," *Ocean Modelling*, vol. 100, pp. 57–77, 2016.

[6] A. Alvarez, A. Caiti, and R. Onken, "Evolutionary path planning for autonomous underwater vehicles in a variable ocean," *IEEE Journal of Oceanic Engineering*, vol. 29, no. 2, pp. 418–429, 2004.

[7] B. Garau, A. Alvarez, and G. Oliver, "Path planning of autonomous underwater vehicles in current fields with complex spatial variability: an a* approach," in *Robotics and Automation, 2005. ICRA 2005. Proceedings of the 2005 IEEE International Conference on*. IEEE, 2005, pp. 194–198.

[8] B. Garau, M. Bonet, A. Alvarez, S. Ruiz, and A. Pascual, "Path planning for autonomus underwater vehicles in realistic oceanic current fields: Application to gliders in the western mediterranean sea," *Journal of Maritime Research*, vol. 6, no. 2, pp. 5–21, 2009.

[9] T. Lee, H. Kim, H. Chung, Y. Bang, and H. Myung, "Energy efficient path planning for a marine surface vehicle considering heading angle," *Ocean Engineering*, vol. 107, pp. 118–131, 2015.

[10] C. Petres, Y. Pailhas, P. Patron, Y. Petillot, J. Evans, and D. Lane, "Path planning for autonomous underwater vehicles," *IEEE Transactions on Robotics*, vol. 23, no. 2, pp. 331–341, 2007.

[11] S. M. LaValle, "Rapidly-exploring random trees: A new tool for path planning," 1998.

[12] C. S. Tan, R. Sutton, and J. Chudley, "An incremental stochastic motion planning technique for autonomous underwater vehicles," *IFAC Proceedings Volumes*, vol. 37, no. 10, pp. 483–488, 2004.

[13] D. Rao and S. B. Williams, "Large-scale path planning for underwater gliders in ocean currents," in *Australasian Conference on Robotics and Automation (ACRA)*, 2009.

[14] T. Fossen, *Handbook of Marine Craft Hydrodynamics and Motion Control*, 2011.

[15] J. H. Moon and H. J. Lee, "Decentralized observer-based output-feedback formation control of multiple unmanned underwater vehicles," *Journal of Electrical Engineering & Technology*, vol. 13, no. 1, pp. 493–500, 2018.

[16] O.-E. Fjellstad and T. Fossen, "Position and attitude tracking of auv's: A quaternion feedback approach," *IEEE Journal of Oceanic Engineering*, vol. 19, no. 4, pp. 512–518, 1994.

[17] B. Subudhi, K. Mukherjee, and S. Ghosh, "A static output feedback control design for path following of autonomous underwater vehicle in vertical plane," *Ocean Engineering*, vol. 63, pp. 72–76, 2013.

[18] F. Alonge, F. D'Ippolito, and F. Raimondi, "Trajectory tracking of underactuated underwater vehicles," *Proceedings of the IEEE Conference on Decision and Control*, vol. 5, pp. 4421–4426, 2001.

[19] A. Aguiar and A. Pascoal, "Dynamic positioning and way-point tracking of underactuated auvs in the presence of ocean currents," *International Journal of Control*, vol. 80, no. 7, pp. 1092–1108, 2007.

[20] F. Repoulias and E. Papadopoulos, "Planar trajectory planning and tracking control design for underactuated auvs," *Ocean Engineering*, vol. 34, no. 11-12, pp. 1650–1667, 2007.

[21] J. Refsnes, A. Sørensen, and K. Pettersen, "Model-based output feedback control of slender-body underactuated auvs: Theory and experiments," *IEEE Transactions on Control Systems Technology*, vol. 16, no. 5, pp. 930–946, 2008.

[22] F. Bi, Y. Wei, J. Zhang, and W. Cao, "Position-tracking control of underactuated autonomous underwater vehicles in the presence of unknown ocean currents," *IET Control Theory and Applications*, vol. 4, 2010.

[23] K. D. Do, "Global tracking control of underactuated odins in three-dimensional space," *International Journal of Control*, vol. 86, no. 2, pp. 183–196, 2013.

[24] X. Xiang, L. Lapierre, C. Liu, and B. Jouvencel, "Path tracking: Combined path following and trajectory tracking for autonomous underwater vehicles," in *2011 IEEE/RSJ International Conference on Intelligent Robots and Systems*. IEEE, 2011, pp. 3558–3563.

[25] P. Encarnaçao and A. Pascoal, "Combined trajectory tracking and path following: an application to the coordinated control of autonomous marine craft," in *Proceedings of the 40th IEEE Conference on Decision and Control (Cat. No. 01CH37228)*, vol. 1. IEEE, 2001, pp. 964–969.

[26] D. Maalouf, A. Chemori, and V. Creuze, "L1 adaptive depth and pitch control of an underwater vehicle with real-time experiments," *Ocean Engineering*, vol. 98, pp. 66–77, 2015.

[27] G. Antonelli, F. Caccavale, S. Chiaverini, and G. Fusco, "A novel adaptive control law for underwater vehicles," *IEEE Transactions on Control Systems Technology*, vol. 11, no. 2, pp. 221–232, 2003.

[28] N. Wang, C. Qian, J.-C. Sun, and Y.-C. Liu, "Adaptive robust finite-time trajectory tracking control of fully actuated marine surface vehicles," *IEEE Transactions on Control Systems Technology*, vol. 24, no. 4, pp. 1454–1462, 2016.

[29] K. Do, J. Pan, and Z. Jiang, "Robust and adaptive path following for underactuated autonomous underwater vehicles," *Ocean Engineering*, vol. 31, no. 16, pp. 1967–1997, 2004.

[30] K. Do and J. Pan, "Robust and adaptive path following for underactuated autonomous underwater vehicles," *Proceedings of the American Control Conference*, vol. 3, pp. 1994–1999, 2003.

[31] G. Antonelli, S. Chiaverini, N. Sarkar, and M. West, "Adaptive control of an autonomous underwater vehicle: experimental results on odin," *IEEE Transactions on Control Systems Technology*, vol. 9, no. 5, pp. 756–765, 2001.

[32] L. Lapierre and B. Jouvencel, "Robust nonlinear path-following control of an auv," *IEEE Journal of Oceanic Engineering*, vol. 33, no. 2, pp. 89–102, 2008.

[33] L. Lapierre, "Robust diving control of an auv," *Ocean Engineering*, vol. 36, no. 1, pp. 92–104, 2009.

[34] R. Cristi, F. Papoulias, and A. Healey, "Adaptive sliding mode control of autonomous underwater vehicles in the dive plane," *IEEE Journal of Oceanic Engineering*, vol. 15, no. 3, pp. 152–160, 1990.

[35] M. Santhakumar and T. Asokan, "Investigations on the hybrid tracking control of an underactuated autonomous underwater robot," *Advanced Robotics*, vol. 24, no. 11, pp. 1529–1556, 2010.

[36] H. Ashrafiuon, K. Muske, L. McNinch, and R. Soltan, "Sliding-mode tracking control of surface vessels," *IEEE Transactions on Industrial Electronics*, vol. 55, no. 11, pp. 4004–4012, 2008.

[37] R. Cui, X. Zhang, and D. Cui, "Adaptive sliding-mode attitude control for autonomous underwater vehicles with input nonlinearities," *Ocean Engineering*, vol. 123, pp. 45–54, 2016.

[38] R. Cui, L. Chen, C. Yang, and M. Chen, "Extended state observer-based integral sliding mode control for an underwater robot with unknown disturbances and uncertain nonlinearities," *IEEE Transactions on Industrial Electronics*, vol. 64, no. 8, pp. 6785–6795, 2017.

[39] T. Elmokadem, M. Zribi, and K. Youcef-Toumi, "Trajectory tracking sliding mode control of underactuated auvs," *Nonlinear Dynamics*, vol. 84, no. 2, pp. 1079–1091, 2016.

[40] S. Liu, Y. Liu, and N. Wang, "Nonlinear disturbance observer-based backstepping finite-time sliding mode tracking control of underwater vehicles with system uncertainties and external disturbances," *Nonlinear Dynamics*, vol. 88, no. 1, pp. 465–476, 2017.

[41] J. Li and P. Lee, "A neural network adaptive controller design for free-pitch-angle diving behavior of an autonomous underwater vehicle," *Robotics and Autonomous Systems*, vol. 52, no. 2-3, pp. 132–147, 2005.

[42] N. Wang and M. J. Er, "Self-constructing adaptive robust fuzzy neural tracking control of surface vehicles with uncertainties and unknown disturbances," *IEEE Transactions on Control Systems Technology*, vol. 23, no. 3, pp. 991–1002, 2015.

[43] K. Ishii, T. Fujii, and T. Ura, "On-line adaptation method in a neural network based control system for auv's," *IEEE Journal of Oceanic Engineering*, vol. 20, no. 3, pp. 221–228, 1995.

[44] F. Zouari, A. Ibeas, A. Boulkroune, J. Cao, and M. M. Arefi, "Adaptive neural output-feedback control for nonstrict-feedback time-delay fractional-order systems with output constraints and actuator nonlinearities," *Neural Networks*, 2018.

[45] F. Zouari, A. Boulkroune, A. Ibeas, and M. M. Arefi, "Observer-based adaptive neural network control for a class of mimo uncertain nonlinear time-delay non-integer-order systems with asymmetric actuator saturation," *Neural Computing and Applications*, vol. 28, no. 1, pp. 993–1010, 2017.

[46] F. Zouari, A. Boulkroune, and A. Ibeas, "Neural adaptive quantized output-feedback control-based synchronization of uncertain time-delay incommensurate fractional-order chaotic systems with input nonlinearities," *Neurocomputing*, vol. 237, pp. 200–225, 2017.

[47] J. Yuh, "A neural net controller for underwater robotic vehicles," *IEEE Journal of Oceanic Engineering*, vol. 15, no. 3, pp. 161–166, 1990.

[48] M. Carreras, J. Yuh, J. Batlle, and P. Ridao, "A behavior-based scheme using reinforcement learning for autonomous underwater vehicles," *IEEE Journal of Oceanic Engineering*, vol. 30, no. 2, pp. 416–427, 2005.

[49] D. Zhu, X. Hua, and B. Sun, "A neurodynamics control strategy for real-time tracking control of autonomous underwater vehicles," *Journal of Navigation*, vol. 67, no. 1, pp. 113–127, 2014.

[50] B. Seok Park, "Neural network-based tracking control of underactuated autonomous underwater vehicles with model uncertainties," *Journal of Dynamic Systems, Measurement and Control, Transactions of the ASME*, vol. 137, no. 2, 2015.

[51] J. Guo, F.-C. Chiu, and C.-C. Huang, "Design of a sliding mode fuzzy controller for the guidance and control of an autonomous underwater vehicle," *Ocean Engineering*, vol. 30, no. 16, pp. 2137–2155, 2003.

[52] N. Wang, Z. Sun, J. Yin, Z. Zou, and S.-F. Su, "Fuzzy unknown observer-based robust adaptive path following control of underactuated surface

vehicles subject to multiple unknowns," *Ocean Engineering*, vol. 176, pp. 57 – 64, 2019.

[53] K. Ishaque, S. S. Abdullah, S. Ayob, and Z. Salam, "A simplified approach to design fuzzy logic controller for an underwater vehicle," *Ocean Engineering*, vol. 38, no. 1, pp. 271–284, 2011.

[54] N. Wang and M. J. Er, "Direct adaptive fuzzy tracking control of marine vehicles with fully unknown parametric dynamics and uncertainties," *IEEE Transactions on Control Systems Technology*, vol. 24, no. 5, pp. 1845–1852, 2016.

[55] L. Merazka, F. Zouari, and A. Boulkroune, "Fuzzy state-feedback control of uncertain nonlinear mimo systems," in *Systems and Control (ICSC), 2017 6th International Conference on*. IEEE, 2017, pp. 103–108.

[56] C. Bechlioulis, G. Karras, S. Heshmati-Alamdari, and K. Kyriakopoulos, "Trajectory tracking with prescribed performance for underactuated underwater vehicles under model uncertainties and external disturbances," *IEEE Transactions on Control Systems Technology*, vol. 25, no. 2, pp. 429–440, 2017.

[57] N. Wang, G. Xie, X. Pan, and S.-F. Su, "Full-state regulation control of asymmetric underactuated surface vehicles," *IEEE Transactions on Industrial Electronics*, 2019.

[58] N. Wang, S. Su, X. Pan, X. Yu, and G. Xie, "Yaw-guided trajectory tracking control of an asymmetric underactuated surface vehicle," *IEEE Transactions on Industrial Informatics*, 2018.

[59] F. Allgöwer, R. Findeisen, and Z. Nagy, "Nonlinear model predictive control: From theory to application," *the Chinese Institute of Chemical Engineers*, vol. 35, no. 3, pp. 299–315, 2004.

[60] C. V. Caldwell, D. D. Dunlap, and E. G. Collins, "Motion planning for an autonomous underwater vehicle via sampling based model predictive control," *OCEANS 2010*, pp. 1–6, 2010.

[61] L. V. Steenson, S. R. Turnock, A. B. Phillips, C. Harris, M. E. Furlong, E. Rogers, L. Wang, K. Bodles, and D. W. Evans, "Model predictive control of a hybrid autonomous underwater vehicle with experimental verification," *Proceedings of the Institution of Mechanical Engineers, Part M: Journal of Engineering for the Maritime Environment*, vol. 228, no. 2, pp. 166–179, 2014.

[62] V. Huynh, M. Dunbabin, and R. Smith, "Predictive motion planning for auvs subject to strong time-varying currents and forecasting uncertainties," *Proceedings - IEEE International Conference on Robotics and Automation*, vol. 2015-June, no. June, pp. 1144–1151, 2015.

[63] L. Medagoda and S. Williams, "Model predictive control of an autonomous underwater vehicle in an in situ estimated water current profile," *Program Book - OCEANS 2012 MTS/IEEE Yeosu: The Living Ocean and Coast - Diversity of Resources and Sustainable Activities*, 2012.

[64] D. Fernandez and G. Hollinger, "Model predictive control for underwater robots in ocean waves," *IEEE Robotics and Automation Letters*, vol. 2, no. 1, pp. 88–95, 2017.

[65] P. Jagtap, P. Raut, P. Kumar, A. Gupta, N. Singh, and F. Kazi, "Control of autonomous underwater vehicle using reduced order model predictive control in three dimensional space," *IFAC-PapersOnLine*, vol. 49, no. 1, pp. 772–777, 2016.

[66] S. Heshmati-Alamdari, A. Eqtami, G. Karras, D. Dimarogonas, and K. Kyriakopoulos, "A self-triggered visual servoing model predictive control scheme for under-actuated underwater robotic vehicles," *Proceedings - IEEE International Conference on Robotics and Automation*, pp. 3826–3831, 2014.

[67] S. Heshmati-Alamdari, G. Karras, P. Marantos, and K. Kyriakopoulos, "A robust model predictive control approach for autonomous underwater vehicles operating in a constrained workspace," *Proceedings - IEEE International Conference on Robotics and Automation*, pp. 6183–6188, 2018.

[68] *Naitonal HF RADAR network - surface currents*. [Online]. Available: http://cordc.ucsd.edu/projects/mapping/maps/

[69] R. Smith, Y. Chao, P. Li, D. Caron, B. Jones, and G. Sukhatme, "Planning and implementing trajectories for autonomous underwater vehicles to track evolving ocean processes based on predictions from a regional ocean model," *International Journal of Robotics Research*, vol. 29, no. 12, pp. 1475–1497, 2010.

[70] B. Allotta, R. Costanzi, F. Fanelli, N. Monni, L. Paolucci, and A. Ridolfi, "Sea currents estimation during auv navigation using unscented kalman filter," *IFAC-PapersOnLine*, vol. 50, no. 1, pp. 13 668–13 673, 2017.

[71] T. Fossen, "Guidance and control of ocean vehicles," *Wiley, New York*, 1994.

[72] D. Koditschek and E. Rimon, "Robot navigation functions on manifolds with boundary," *Advances in Applied Mathematics*, vol. 11, no. 4, pp. 412–442, 1990.

[73] G. Pin, D. Raimondo, L. Magni, and T. Parisini, "Robust model predictive control of nonlinear systems with bounded and state-dependent uncertainties," *IEEE Transactions on Automatic Control*, vol. 54, no. 7, pp. 1681–1687, 2009.

[74] E. F. Camacho and C. B. Alba, *Model predictive control*. Springer Science & Business Media, 2013.

[75] D. Limon, T. Alamo, D. M. Raimondo, D. M. de la Peña, J. M. Bravo, A. Ferramosca, and E. F. Camacho, *Input-to-State Stability: A Unifying Framework for Robust Model Predictive Control*. Berlin, Heidelberg: Springer Berlin Heidelberg, 2009, pp. 1–26.

[76] D. L. Marruedo, T. Alamo, and E. Camacho, "Input-to-state stable mpc for constrained discrete-time nonlinear systems with bounded additive uncertainties," *41st IEEE Conf. Decision and Control*, pp. 4619 – 4624, 2002.

[77] G. C. Karras, P. Marantos, C. P. Bechlioulis, and K. J. Kyriakopoulos, "Unsupervised online system identification for underwater robotic vehicles," *IEEE Journal of Oceanic Engineering*, pp. 1–22, 2018.

[78] S. Garrido-Jurado, R. M. noz Salinas, F. Madrid-Cuevas, and M. Marín-Jiménez, "Automatic generation and detection of highly reliable fiducial markers under occlusion," *Pattern Recognition*, vol. 47, no. 6, pp. 2280 – 2292, 2014.

[79] M. Quigley, B. Gerkey, K. Conley, J. Faust, T. Foote, J. Leibs, E. Berger, R. Wheeler, and A. Ng, "Ros: an open-source robot operating system," in *Proc. of the IEEE Intl. Conf. on Robotics and Automation (ICRA) Workshop on Open Source Robotics*, Kobe, Japan, May 2009.

[80] S. G. Johnson, "The nlopt nonlinear-optimization package, http://ab-initio.mit.edu/wiki/index.php/nlopt."

[81] V. Asouti, X. Trompoukis, I. Kampolis, and K. Giannakoglou, "Unsteady cfd computations using vertex-centered finite volumes for unstructured grids on graphics processing units," *International Journal for Numerical Methods in Fluids*, vol. 67, no. 2, pp. 232–246, 2011.